Neural interface engineering for electrophysiology application

by

Hyungsoo Kim

A dissertation submitted in partial fulfillment of

the requirement for the degree of

Doctor of Philosophy

(Electrical Engineering)

at the

UNIVERSITY OF WISCONSIN-MADISON

2018

Date of final oral examination: 8/27/2018

The dissertation is approved by the following members of the Final Oral Committee:

Dr. Zhenqiang (Jack) Ma, Advisor, Electrical and Computer Engineering
Dr. Justin C. Williams, Biomedical Engineering
Dr. Hongrui Jiang, Electrical and Computer Engineering
Dr. Samuel O. Poore, Surgery
Dr. Erik W. Dent, Neuroscience
Dr. Zongfu Yu, Electrical and Computer Engineering

To my dear Parents, Wife, Son and Grandma,

Jiyoun, Jaeheon, Hyesook, Dowook and Heungsum,

their unconditional support and love

Acknowledgments

It has been a wonderful experience filled with countless fond memories that I have had while studying here in Madison. I have been working and studying very hard to reach my goal, and finally I am about to get it achieved. During this remarkable journey, I have met many great people who helped me improve myself and contribute to develop my academic strength.

First and foremost, I would like to thank my advisor, Professor Zhenqiang Ma, for his academic and professional guidance. It has been a blessed but challenging experience working in his lab, and he has made unconditional support to help me improve and grow as a scientist and academic professional.

I would also like to thank Professor Justin C. Williams, one of my committee members as well as co-advisor, for his expertise knowledge and insightful advice to research that I have been working. I will never forget the memories working with NITRO lab. Members, Jared P. Ness, Sarah Brodnick and Joseph Novello.

And I could not tell my research stories without the working experiences in Dent Lab. I sincerely would like to thank Professor Erik W. Dent and his lab members, Karl Richers and Kendra Taylor.

In addition, I would like to express my appreciation to Professor Samuel O. Poore and Dr. Aaron M. Dingle. Samuel has provided me with much support and confidence during my years at Madison. I will not forget one of my best friend, Aaron with his positive attitude and valuable discussions we made for our project.

Above all, I would like to thank all of the past and present members of the Ma Lab who have helped me countless times and in almost every way imaginable over the past 4 years.

I would not complete my doctorate without the help and friendship of my colleagues. In particular, Dr. Dongwook Park, my old friend, allowed me to participate in his experiments when I first joined the lab and taught me the device fabrication and electrophysiology. I would also like to thank Jihye Bong who has helped me in many ways. I would like to thank Dr. Junghun Seo, Dr. Munho Kim, Namki Cho, Subin Lee, Dr. Minkyu Cho, Dr. Jaesung Lee, Dr. Yeihwan Jung, Dr. Dongjun Kim, Juhwan Lee, Dr. Kwangeun Kim. Special thanks go to Inkyu Lee for his dedication to the project that we were pursuing together. I couldn't make it without his contribution. I will never forget the time we spent together in Madison.

I have been very fortunate to have such supportive and reliable thesis committee members, Professor Hongrui Jiang and Professor Zongfu Yu, for their comments on my manuscript and their participation in my thesis defense.

Finally, I would like to thank my family for all the love and support you have given me and continue to give me throughout my life. Special thanks goes to my wife, Jiyoun Yoon. Jiyoun has been my greatest blessing in my life. When I lost my way in the darkness and was wandering, she was resolute and encouraged me to get back up again. I would like to thank my lovely son, Jaeheon. He is the source of power that can keep me running even in hard times. Most importantly, I sincerely thank my father and mother, Dowook Kim and Hyesook Shin. Without your unconditional support and love, I couldn't do anything. Because of you, I never quit. Lastly, I would like to attribute this glory to my grandmother in heaven.

I would like to acknowledge the following funding agencies who provided the financial support for my doctoral research: ARO (W911NF-14-1-0652), NIH (R01 HG000225), NSF (DMR-1124131), DOE (DE-NA0002915) and DARPA (managed by ONR: NW911NF-14-1-0652).

List of publications in refereed journals

1. H. Kim, I. Lee, *et al*. Single-neuronal cell culture and monitoring platform using a fully transparent microfluidic DEP device. *Sci. Rep*., In Press
2. H. Kim, A.M. Dingle, *et al*. The novel combination of cuff and sieve electrodes (CASE) for bi-directional peripheral nerve interfacing.
3. Park, D.W., Kim, H., Bong, J., Mikael, S., Kim, T.J., Williams, J.C. and Ma, Z., 2016. Flexible bottom-gate graphene transistors on Parylene C substrate and the effect of current annealing. *Applied physics letters*, 109(15), p.152105.
4. Park, D.W., Brodnick, S.K., Ness, J.P., Atry, F., Krugner-Higby, L., Sandberg, A., Mikael, S., Richner, T.J., Novello, J., Kim, H. and Baek, D.H., 2016. Fabrication and utility of a transparent graphene neural electrode array for electrophysiology, in vivo imaging, and optogenetics. *Nature protocols*, 11(11), p.2201.
5. Park, D.W., Ness, J.P., Brodnick, S.K., Esquibel, C., Novello, J., Atry, F., Baek, D.H., Kim, H., Bong, J., Swanson, K.I. and Suminski, A.J., 2018. Electrical neural stimulation and simultaneous in vivo monitoring with transparent graphene electrode arrays implanted in GCaMP6f mice. *ACS nano*, 12(1), pp.148-157.

Introduction

The brain is a wondrous and complex organ, a biological machine forged by the evolutionary forces of nature. The human brain contains 100 billion neurons and each neuron is connected by synapses to several thousand other neurons. Connected neurons work together to produce perceptions and sensations, memories and emotions, physical movements and abstract constructs. The neurons communicate by means of electricity that passes along and across their cellular membrane. Much of what is known about brain physiology is through the measurement of this electrical activity, either with relatively large electrodes placed on the scalp or tiny microelectrodes inserted into the brain tissue itself. At the finer end of this scale, scientists have discovered much about the way individual neurons extract sensory information, adapt their behavior to form a memory, and convey signals to other regions of the brain. However, it has long been recognized that the brain operates on a global scale, through the collective behavior and interaction of its neural units[1]. Information is processed in several regions of the brain simultaneously, and the activity of neighboring neurons can be quite different from one another. By one analogy, the attempt to assess brain function by observing a single neuron is like looking at the output of one transistor to learn how a computer works. Thus, the recording of many neurons simultaneously is necessary to truly reveal the mechanisms of the brain[2]. In recent decades, a variety of recording techniques have been developed for a neural interface such as electroencephalography (EEG), magneto-encephalography (MEG), electrocorticography (ECOG), local field potential (LFP) recordings, micro-electrode array (MEA) and peripheral nerve interfaces (PNIs) to the micron-level precision required for multi-neuron recording. Their small size allows many recording channels to be placed onto one device.

One of the goals of neural interface research is to create a seamless connection between the nervous system and the neuroprostheses either by stimulating or by recording from neural tissue to restore or substitute function for individuals with neurological deficits or disabilities. Hence, significant amount of scientific and technological efforts have been devoted to develop neural interfaces that link the nervous system with robotic prosthetic devices. The creation of a novel neural interface is essential for developing the full potential of advanced prosthesis technology required to replace lost limbs. Additionally, meticulous studies of a single neuron and between neurons utilizing the neural interface technology should be made to elucidate fundamental biological phenomena such as cellular processes and heterogeneities. Particularly, an electrophysiological study of neural networks can provide knowledge to unravel the functions of brain. When fundamental research about molecular and cellular mechanisms of a single neuron and electrophysiological studies using neural interfaces on both the central and peripheral nervous systems are done together, it has a synergistic effect on neural interface technology.

The research and methodologies described in this dissertation stem from our research group's efforts to optimize the design and expand the applications of neural interfaces. The dissertation is organized into four chapters. Chapter 1 is a review of neural interface technology and study of neural signal detection. This chapter provides a foundation for Chapter 2 and 3. Chapter 2 is a study of a neural interface as cellular level research. We present an advanced single-neuronal cell culture and monitoring platform using a fully transparent microfluidic dielectrophoresis (DEP) device for unabated monitoring of neuronal cell development and function. The device is mounted inside a sealed incubation chamber to ensure improved homeostatic conditions and reduced contamination risk. Consequently, we

successfully trap and culture single neurons on a desired location and monitor their growth process over a week. Chapter 3 deals with the specific application of PNIs to the sciatic nerve of a rat as a nervous system-level research. We developed novel devices, “cuff and sieve electrodes” (CASE), that integrate microfabricated cuff and sieve electrodes capable of broad (*via* cuff) and precise (*via* sieve) selectivity to increase the strengths and simultaneously decrease the weaknesses of traditional electrode designs. We performed terminal device implantations in a rat sciatic transection and repair model to test the capacity of the CASE interface. The sciatic nerve was stimulated by the sieve portion of the CASE electrode and somatosensory evoked potentials were recorded from the somatosensory cortex via micro-eletrocorticography. The ability to elicit cortical responses from sciatic nerve stimulation demonstrates the proof of concept for both the implantation and chronic monitoring of CASE interfaces for innovative prosthetic control. Lastly, in Chapter 4, I will identify areas in which further investigation is needed and propose future directions of both cellular and system-level neural interface.

List of Tables

List of Figures

Table of Contents

Chapter 1

Neural interface technology

1.1 Neural interfacing

Neural interfaces can be used to implement sensorimotor neuroprostheses, to map epileptic neural activity, and to study systems neuroscience more generally in animal models. The technological approaches can be tailored to interfaces at various levels of the central and peripheral nervous systems, from individual neurons to the superimposed activity of neural populations.

1.1.1 Neural interfacing with the central nervous system

The central nervous system (CNS) is the part of the nervous system which is comprised of the brain and spinal cord. The CNS receives information from sensory nerve extremities and in return controls the function of muscles throughout the body. The nerves conducting this information are made of bundles of tightly packed axons, each leading to a different neuron in the peripheral nervous system (PNS) or the CNS. In case of traumatic injury, however, the axons in motor pathway hardly regenerate and partial or total paralysis can occur. One of the leading applications for BCI devices is the development of neuroprosthetics to allow direct connection of sensory and motor brain function to a computer. Most of the neurons of the CNS are located in the cerebral cortex, a thin convoluted neural layer at the surface of the forebrain[3], making them readily accessible by surface interfacing devices. The cerebral cortex has specialized areas that control sensory,

motor function, visual, auditory, language, comprehension, speech, memory, awareness and consciousness. It is the electrical characteristics of the central nervous system and its connectivity that interests the researchers and allows us to design the innovative devices and methods to interface with this complex system. Measuring these signals has been a goal for developing research (and now also commercial) brain-interfacing tools, such as the well known electroencephalogram (EEG) which can record the brain activity along the scalp[4]. However, as the electrical fields produced are very small, decay rapidly and contain important spatial information, more accurate interfacing devices have been developed such as the electrocorticogram (ECoG) which can record brain activity directly from cerebral cortex[5]. More recently, this approach has been improved using flexible thinfilm micro-fabrication techniques to create a less invasive high-resolution electrode array called micro-ECoG [6]. Micro-ECoG technology is still in its infancy, and while significant improvements have been accomplished in the fabrication of flexible electrodes for this application, a lot remains to be understood about the material interaction with the brain, particularly in the context of chronic implantation. These devices have multiple applications, from providing a communication interface for paralyzed patients, monitoring or predicting epileptic seizures, or controlling computer interfaces. In addition, some brain interface devices rely on recording of an evoked activity in CNS after stimulation of sensory function to evaluate their proper function. The two main categories of neural interfaces for the CNS are near-field CNS measurements and far-field CNS measurements. The near-field extracellular CNS measurements are performed by amplifying the potential difference between a microelectrode tip implanted in the cortex and a reference electrode located within a few millimeters. The far-field CNS measurements record the electric potential sub-durally, epi-

durally or on the scalp. The recorded signals can be divided in two components, one is the local field potential (LFP) which measures coherent low frequency changes in the membrane potential (<300 Hz) associated with synaptic current of many neurons and the other is higher frequency signal (300 Hz-10 kHz) consisted of multi-unit activity resulting from action potential of nearby neurons. The different frequency components represent the different spatial ranges, up to 100 μm for single-unit signals, hundreds of microns for multi-unit signals and a few millimeters for local field potential (LFP). Devices such as the micro-electrocorticogram (micro-ECoG), the electroencephalogram (EEG) are typically used for measuring these signals, with varying efficacies.

1.1.2 Neural interfacing with the peripheral nervous system

PNS is one of two components that make up the nervous system. The main function of the PNS is to connect the CNS to limbs and organs. The peripheral nervous system is divided into the somatic nervous system, and the autonomic nervous system. The somatic nervous system is under voluntary control, and transmits signals from the brain to end organs such as muscles. The sensory nervous system is part of the somatic nervous system and transmits signals from senses such as taste and touch (including fine touch and gross touch) to the spinal cord and brain. The autonomic nervous system is a 'self-regulating' system which influences the function of organs outside voluntary control, such as the heart rate, or the functions of the digestive system.

Peripheral nerve injuries are serious health problems that can lead to loss of sensation and mobility, as the resulting loss of innervation impairs voluntary muscle movements and normal sensation. In Europe more than 300, 000 cases of peripheral nerve

injuries occur annually and in the United States, 360, 000 people suffer from upper extremity paralytic syndromes on an annual basis[7,8]. In recent years, many scientific and technological efforts have been devoted to develop hybrid bionic systems that link, via neural interfaces, the human nervous system with electronic and/or robotic prostheses, with the main aim of restoring motor and sensory functions in patients with spinal cord injuries, brain injuries, or degenerative diseases. A number of neuroprostheses, developed to artificially substitute or mimic sensorimotor functions in patients with neurological impairment, include interfacing the PNS or muscles by means of appropriate electrodes, which may allow neuromuscular stimulation and neural signal recording. Recent developments in the technology of electronic implants and in the understanding of neural functions have also made feasible the construction of interfaces that work by bi-directionally interchanging information between the CNS and computerized artificial instruments, by means of microwire or microelectrode arrays implanted in the brain[9] or in the spinal cord[10]. Considering the application of different types of electrodes, the desired selectivity of stimulation or recording from individual nerve fibers or motor units increases in parallel with the invasiveness of the electrode implantation (Fig. 1.1). For example, surface and muscular electrodes can record EMG activity from and stimulate only the underlying or implanted muscles. Extraneural electrodes, such as cuff and epineurial electrodes, provide simultaneous interface with many axons in the nerve, whereas intrafascicular and sieve electrodes inserted in the nerve may interface small groups of axons within a nerve fascicle. On another hand, the state of the nerve varies; cuff and intrafascicular electrodes can be applied to intact nerves in acute or chronic studies,

whereas, by definition, regenerative sieve electrodes are implanted in transected nerves that need to regenerate across the electrode sieve over several months.

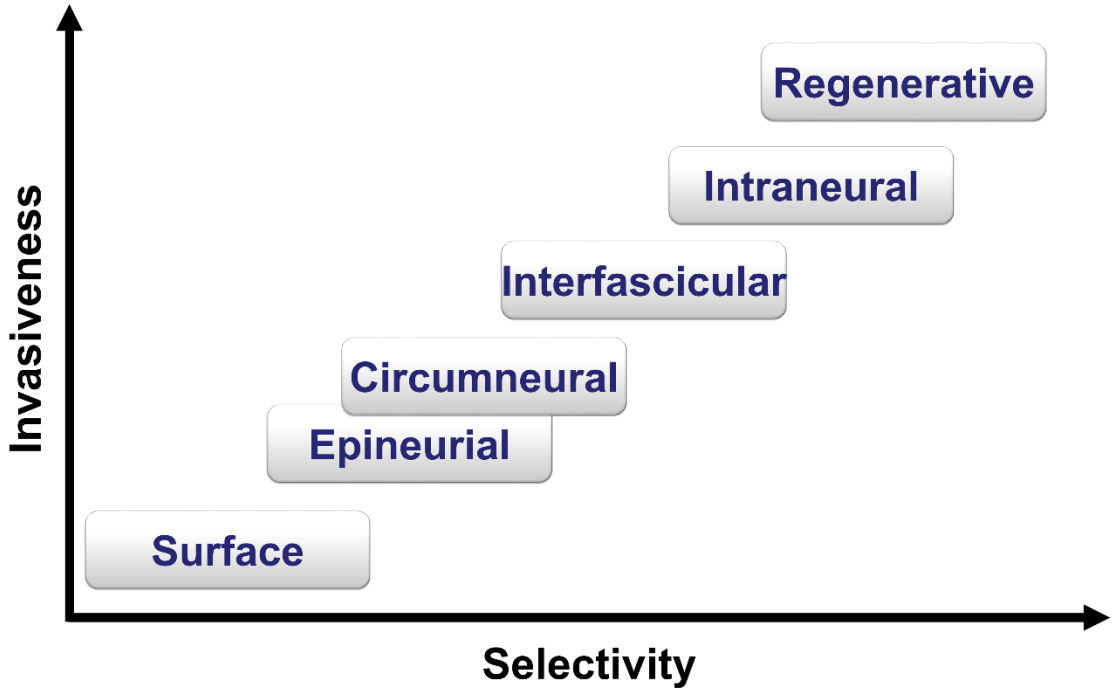

Figure 1.1. The different types of PNIs. PNIs can be categorized into several types based on levels of invasiveness and selectivity. This represents a general classification, despite that selectivity actually depends on the type of nerve and anatomical and physiological considerations for each particular application.

1.2 Neural signal detection

1.2.1 Electrical activity in the brain

Cell-to-cell signaling in the nervous system arises through the movement of charged ions through specialized channels in the cellular membrane. The charged particles – sodium,

potassium, and chloride being the most important species of ions – bring about voltage changes in the cells through which they flow. Occasionally, a single voltage transient known as an action potential occurs. The pattern of pulse-like action potentials that a brain cell, or neuron, elicits is the method of signaling in the brain. An action potential from one neuron, for instance, may cause a connected neuron to generate an action potential, and so on. An action potential, or "spike", is detectale as a rapid voltage change occurring inside of a neuron. In laboratory studies, this voltage change is measured with a very fine micro-electrode, usually made of glass, inserted through the cell membrane[11]. As shown in Fig. 1.2, the initail upswing of an intracellularly recorded action potential waveform corresponds to an influx of sodium ions (Na^+), which is following by a slower efflux of potassium ions (K^+). Note that the positive-going phase of the spike lasts about 1ms, and the entire action potential spans 80-90 mV.

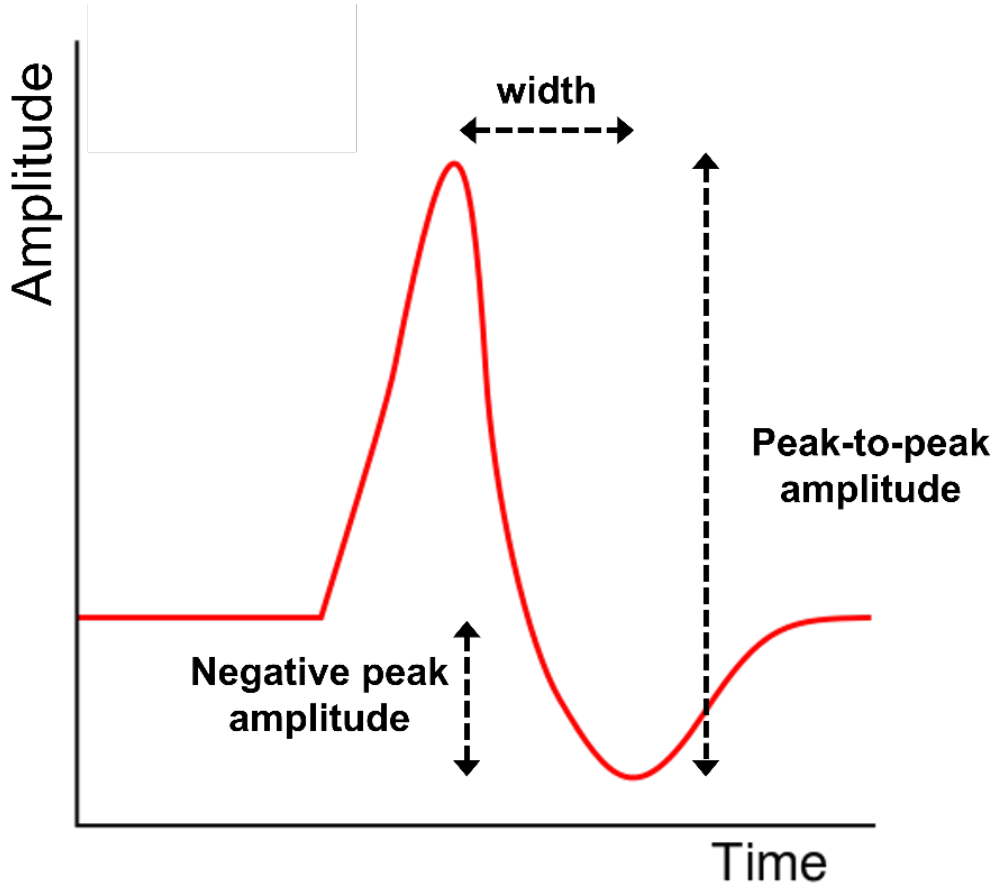

Figure 1.2. Extracellular action potential, also called a "spike".

The occurrence of an action potential can be inferred through the detection of electrical current flowing in the tissue outside the neuron. This extracellular current exists as a counterpart to the intracellular ionic current, forming a closed circuit that allows the action potential to take place. The preferred method of detecting action potentials extracellularly is with a fine metal micro-electrode[12]. The metal forms a capacitive coupling to the aqueous tissue medium, allowing it to detect changes in the in the potential field created by action potential currents. Traditionally, metal micro-electrodes are made from stainless steel, tungsten, or platinum wire. An example of an extracellular spike is

shown in Fig. 1.2. Detecting action potentials extracellularly circumvents the need of cell impalement, an often laborious technique that can damage the cell membrane.

1.2.2 Recording from multiple neurons

One additional advantage of extracellular electrodes is their ability to record from multiple neurons in the vicinity of the electrode tip. Intracellular electrodes cannot record from more than one neuron, and maintaining impalements with multiple electrodes is extremely difficult, even when the brain tissue is immobilized in a petri dish. An abundance of local neural activity, however, means that extracellularly recorded spikes must be assigned to their respective neural sources in order for meaningful single-unit spike analysis to take place. This task is confounded by the possibility that two or more spikes may overlap in time. Moreover, distant neurons contribute to the voltage fluctuations at the tip, appearing as random noise. The identification of multiple-unit action potentials, then, becomes a challenging problem of signal detection and classification. Many spike classification methods have been developed over the years[13]. The underlying principle of these methods is that spikes produced by one nearby neuron have a different amplitude and shape than those produced by another neuron. The characteristic appearance of a spike waveform is a result of many factors: the cellular mechanisms generating the action potential, the neuron-electrode and surrounding conductive tissue. Some typical features of an extracellularly recorded spike are indicated in Fig. 1.2.

1.3 Thin-film neural interface device fabrication methods

The development of thin film neural devices has been largely based on the innovations made in microfabrication techniques, used in many other applications including electronics devices. Amongst the various materials available, two are of particular interest in the context of thin film neural devices, polyimide and parylene C. To be considered as a thin-film neural interface device substrate, the polymer has to possess good dielectric property, moisture uptake resistance, chemical resistance, biocompatible and excellent mechanical properties. These two materials have distinctive properties that make them suitable for different applications. Polyimide is one of the most commonly available polymers that has excellent moisture and electrical insulation properties and if flexible. Currently there are different types of polyimide polymers available in the market, but the photodefinable polyimide is the preferred choice due to its simplicity in microfabrication that does not require hazardous chemicals, such as Hydrofuric Acid (HF) for the etching process. Parylene C is one of the first and few materials that have been approved by the FDA for chronic implant devices. It also has higher light transmission property than polyimide and looks transparent. The detailed electrode fabrication process is described in the following chapter.

Chapter 2

Single-neuronal cell culture and monitoring platform using a fully transparent microfluidic DEP device

2.1 Abstract

Dielectrophoresis using multi-electrode arrays allows a non-invasive interface with biological cells for long-term monitoring of electrophysiological parameters as well as a label-free and non-destructive technique for neuronal cell manipulation. However, experiments for neuronal cell manipulation utilizing dielectrophoresis has been constrained because dielectrophoresis devices generally function outside of the controlled environment (*i.e.* incubator) during the cell manipulation process, which is problematic because neurons are highly susceptible to the properties of the physiochemical environment. Furthermore, the conventional multi-electrode arrays designed to generate dielectrophoretic force are often fabricated with non-transparent materials that confound live-cell imaging. Here we present an advanced single-neuronal cell culture and monitoring platform using a fully transparent microfluidic dielectrophoresis device for the unabated monitoring of neuronal cell development and function. The device is mounted inside a sealed incubation chamber to ensure improved homeostatic conditions and reduced contamination risk. Consequently, we successfully trap and culture single neurons on a desired location and monitor their growth process over a week. The proposed single-neuronal cell culture and monitoring platform not only has significant potential to realize an *in vitro* ordered neuronal network,

but also offers a useful tool for a wide range of neurological research and electrophysiological studies of neuronal networks.

2.2 Introduction

Single-cell analysis has attracted an increasing amount of attention over the past decades, and paves the way for elucidating fundamental biological phenomena such as cellular processes and heterogeneities[14-17]. Of particular importance to the field of neuroscience, meticulous studies of single neurons and between spatially isolated neurons provide a better understanding of the dynamics of functional neuronal networks as well as their fundamental molecular and cellular mechanisms. Also, elucidating the link between neural activity and sensation or motor control remains major challenges. This research is essential to push forward personalized treatments of neurological disorders including epilepsy, Parkinson's disease, Alzheimer's disease, and other cognitive and motor disorders.

To date, various cell manipulation techniques such magnetophoresis, optical tweezers, acoustic means, and dielectrophoresis (DEP) [18], have been explored for the field of single-cell analysis. Among these techniques, DEP, an electrokinetic phenomenon acting on polarizable particles in a non-uniform electric field, benefits from the fact that cells can be trapped, aligned and patterned without requiring additional elements (*i.e.* optical device, magnet and light source)[19-26]. Moreover, DEP provides a healthy environment for neurons to reside by incorporating electrode structures that are designed to minimize the electric field intensity[27].

Nevertheless, the availability of DEP for realizing an *in vitro* cultured neuronal network is limited by the difficulty of the neuron cultures, which are highly susceptible to

the properties of the physiochemical environment (*i.e.* pH, osmotic pressure, humidity, and temperature) and infection[28-31]. In addition, imaging the morphology and activity of cultured neurons using inverted microscope is often confounded by the use of non-transparent electrodes and substrate[28-30,32].

Here, we propose an advanced single-neuronal cell culture and monitoring platform using a fully transparent microfluidic DEP device. This device consists of multi-electrode arrays (MEAs) made of indium-tin-oxide (ITO) and a PDMS microfluidic chip. To reduce the risk of culture contamination, the device was mounted inside an incubated microscope system. A target neuron was trapped and released sequentially by an array of ring-shaped electrodes arranged in a row to demonstrate the capabilities of the proposed system. Consequently, we were able to successfully culture and monitor single-neuronal cells over time. This advanced platform for trapping of single-neuronal cells and monitoring of its electrophysiological parameters enables novel and detailed neurological studies.

2.3 Theory

2.3.1 Dielectrophoresis

DEP is a translational motion of polarizable particles suspended in a medium induced by a non-uniform electric field[18,22]. The behavior of neutral body should be carefully distinguished from motion cause by the response to free charge on a body in an electric field. In a uniform electric field, a charged particle is attracted to the electrode of opposite polarity but a neutral body will just be polarized in the same field (Fig. 2.1a). We can observe different behavior of the neutral, polarizable body in a nonuniform electric field (Fig. 2.1b). The charged one still attracted to the electrode of opposite polarity electrode.

In this case, a translational force is exerted on the neutral, polarizable body and it pulled toward region of high electric field intensity. In fact, the two charges on the body are equal because the particle is neutral. But the fields operating on the two regions are unequal. This uneven electric field intensity on each side of the polarized particle gives rise to a net force.

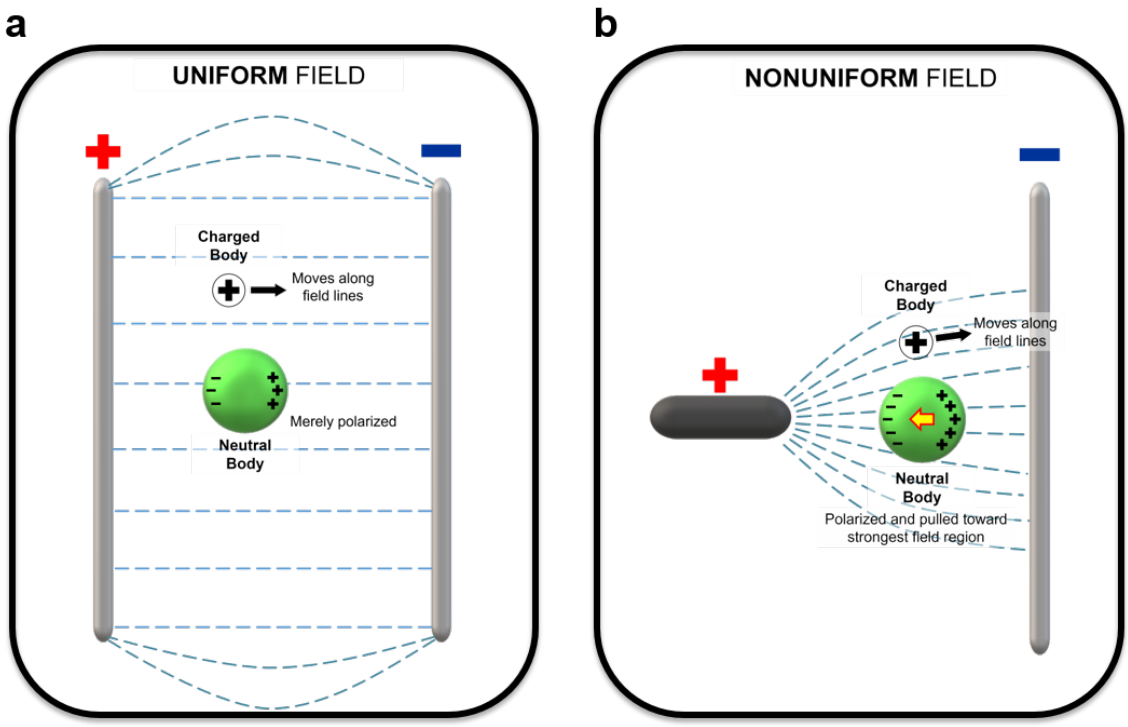

Figure 2.1. Behaviors comparison of neutral body and charged body. (**a**) Neutral and charged body in uniform field. (**b**) Neutral and charged body in nonuniform field.

In Fig. 2.1, we have not specified which electrode is positive or negative when the force is induced on neutral body under the nonuniform field. It does not matter in the case of neutral body. The force upon the neutral, polarizable body in the nonuniform field is normally in the same direction no matter which electrode is charged positive or negative (Fig. 2.2).

That is the reason why we can apply the AC signal to generate a dielectrophoretic force. As shown in Fig. 2.2, positively charged particle is attracted to the negative electrode while polarized neutral body moves towards the region of highest field intensity.

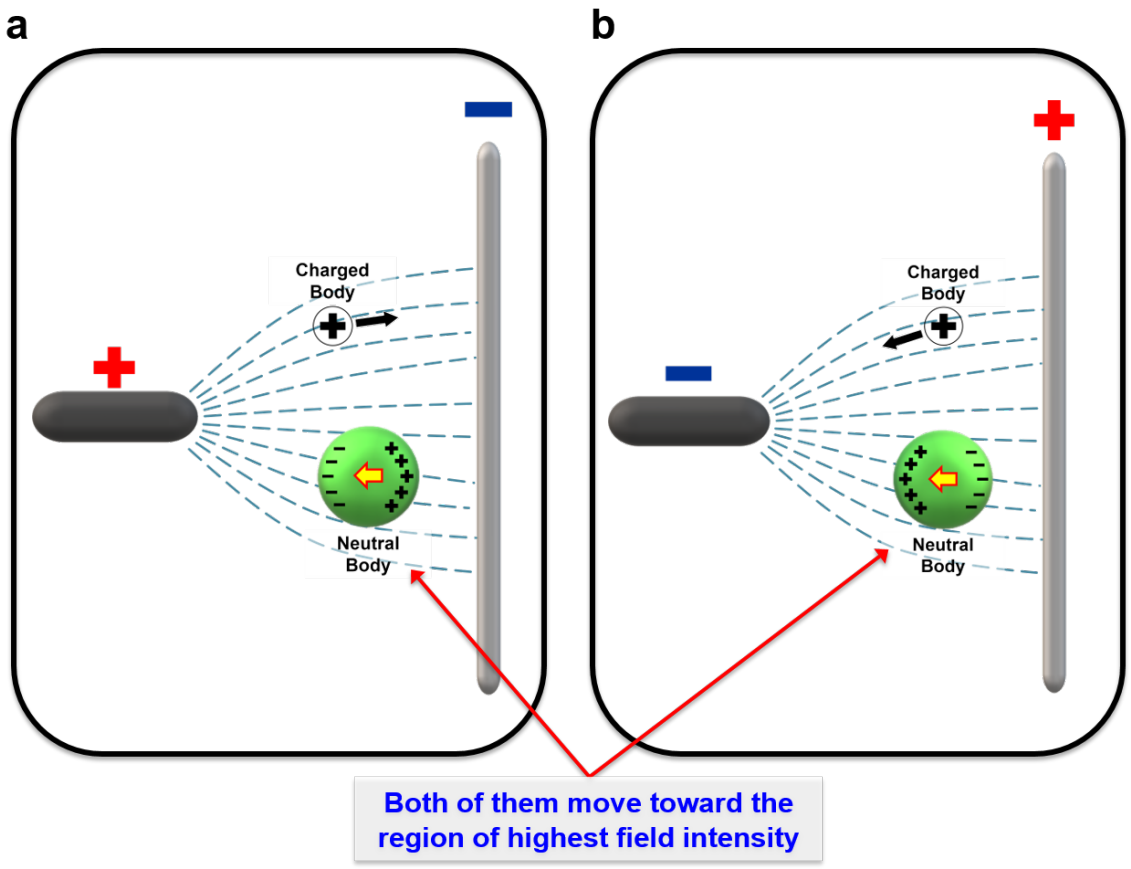

Figure 2.2. Behaviors comparison of neutral and charged body in an nonuniform electric field. Highest electric field intensity region: (**a**) positive electrode, (**b**) negative electrode. Both of cases, neutral bodies are attracted to the highest field intensity region.

The resulting force felt by the particle is due to an induced dipole as described by the Maxwell-Wagner (MW) theory[33,34]. The dielectrophoretic force on a sphere can be derived

directly from the induced dipole model. The time-averaged DEP force on a particle in a non-uniform electric field can be expressed as

$$\vec{F}_{DEP} = 2\pi R^3 \varepsilon_m \mathrm{Re}[f_{CM}(\omega)] \nabla \vec{E}_{rms}^2 \quad (1)$$

where R is the radius of the particle, ε_m is the relative permittivity of the surrounding medium, $\mathrm{Re}[f_{CM}(\omega)]$ is the real part of the Clausius-Mossotti (CM) factor, ∇ is the del vector operator, and E_{rms} is the root-mean-square value of the applied electric field[22]. For the case of a spherical, homogeneous particle of permittivity ε_p, the CM factor which describes the effective polarizability of the particle which varies with the applied frequency[33] is given by

$$f_{CM}(\omega) = \frac{\varepsilon_p^* - \varepsilon_m^*}{\varepsilon_p^* + 2\varepsilon_m^*} \quad (2)$$

where ε_p^* and ε_m^* are the complex permittivities of the particle and the medium, respectively, with $\varepsilon_p^* = \varepsilon_p - j\frac{\sigma_p}{\omega}$, and $\varepsilon_m^* = \varepsilon_m - j\frac{\sigma_m}{\omega}$ where ε_p and ε_m are the permittivities of the particle and the medium, respectively, σ_p and σ_m are the conductivities of the particle and the medium, respectively, and ω is the angular frequency of the applied electric field. The real part of the CM factor ($\mathrm{Re}[f_{CM}(\omega)]$) has a value between -0.5 and 1 and determines the direction of the DEP force. When the particles that are more polarizable than the surrounding media, the $\mathrm{Re}[f_{CM}(\omega)]$ is positive and the particles are attracted to the regions of electric field intensity maxima, positive dielectrophoresis (pDEP), whereas when the particles that are less polarizable than the media, $\mathrm{Re}[f_{CM}(\omega)]$ is negative and the particles move toward electric field intensity minima (*i.e.* repelled from field maxima), negative dielectrophoresis (nDEP). The

calculation result of the real part of the Clausius-Mossotti factor (f_{CM}) is shown in Fig. 2.3. The result plot as s function of frequency by using a neuronal single-shell model [35]. The parameters for the single-shell model of neuronal cell were shown in Table 1. In our experiment, conductivity of neuronal cell culture medium is 1.2 S/m, as the working solution for manipulating neurons.

Table 1. Parameters for the single-shell model of cortical rat neuron

Parameter	Value
Cytoplasm permittivity	7.1×10^{-10} F/m
Cytoplasm conductivity	0.75 S/m
Membrane permittivity	1.8×10^{-12} F/m
Membrane conductivity	1×10^{-7} S/m
Medium permittivity	7.1×10^{-10} F/m

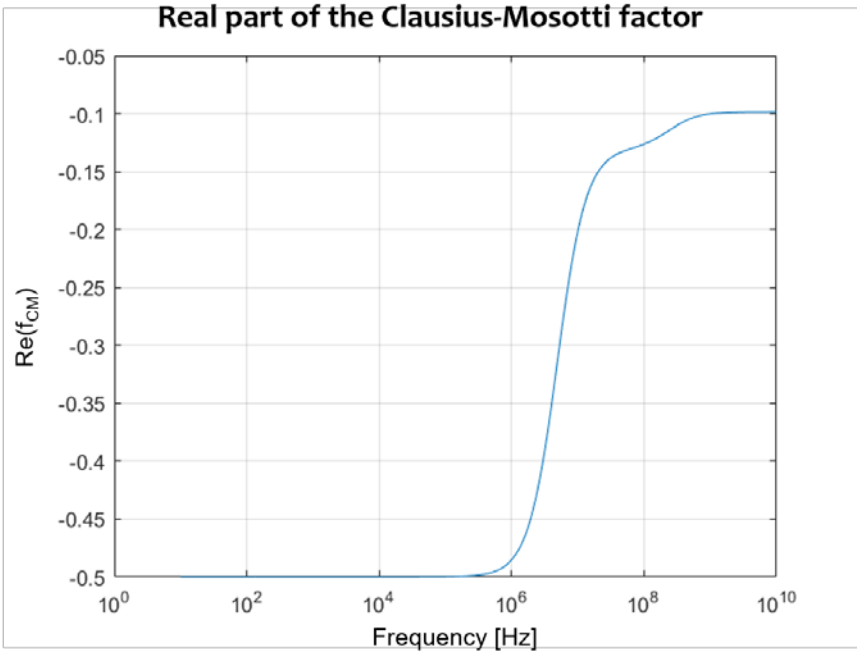

Figure 2.3. Real part of the Clausius-Mosotti factor as a function of frequency for a cortical neuron. The curve was calculated for a medium conductivity: σ_m=1.2 S/m.

As we can see in Fig. 2.3, nDEP will occur over the entire frequency range up to very high frequencies. For neuroscience applications, the nDEP is better suited as it makes possible the use of commonly used neuronal cell culture media due to the conductivity and permittivity of the media being higher than those of neurons [19,20,30] as well as allows neurons to reside in a healthy environment by attracting the neurons to the region of electric field intensity minima.

2.3.2 Transmembrane potential

A transmembrane potential may be induced when cells are exposed to an electric field. This potential changes with the magnitude and frequency of the electric field, and when it reaches a certain level, breakdown of the cellular membrane will occur [36]. According

to the single-shell model, assume a cell can be represented as a homogeneous sphere surrounded by a thin shell. Neglecting the membrane conductivity, membrane thickness and resting membrane potential, when an alternating (sinusoidal) electric field is applied, the induced transmembrane potential Vm can be simplified as Marszalek et al. (1990) [37]:

$$V_m = \frac{1.5\left|\vec{E}\right| R cos\alpha}{\sqrt{1+(2\pi f\tau)}} \quad (3)$$

where α represents the angle between the electric field line and a normal from the center of the sphere to a point of interest on the membrane (the maximal transmembrane potential is induced at the membrane patch facing an electrode, $\alpha = 0^{\circ}$ or 180°); and τ is the time constant of the membrane, which can be written as:

$$\tau = R_{mem} C_{mem} \left(\frac{1}{\sigma_i} + \frac{1}{2\sigma_m} \right) \quad (4)$$

where R_{mem} and C_{mem} represent the specific membrane resistance and capacitance per unit area; and σ_i represents the conductivity of the cytoplasm. Transmembrane value, V_m, have an important impact on the viability of the neurons manipulated by nDEP forces, and a lower transmembrane potential is desirable.

2.4 Materials and methods

2.4.1 Fabrication of fully-transparent microfluidic DEP device

The proposed fully-transparent microfluidic DEP device is composed of the MEAs integrated glass substrate and microfluidic chip [38]. The fabrication process is described with schematic illustrations in Fig. 2.4a. The fabrication began with ITO deposition and patterning. A 250 nm thick ITO film with a sheet resistance of 6 Ω/□ was deposited on a clean glass substrate by radio frequency (RF) magnetron sputtering at room temperature. Then, a photolithography and wet-etching processes using hydrochloric acid (HCl) and buffered oxide etchant (BOE) solution were carried out to define the ring-shaped trap electrode and counter electrodes. A bilayer of Ti (20nm)/Au (200nm) was deposited using an electron beam evaporator to serve as the pad electrode for making a connection between the DEP device and the signal generator (Fig. 2.4a). Then, a dielectric insulator (SiO_2) with a thickness of 200 nm was deposited by an electron-beam evaporator and patterned by the wet-etching process to define the pad electrodes. The internal diameter and the width of the ring-shaped electrode were 40 μm and 20 μm, respectively. The gap between the ring electrode and the ground plane was 20 μm. Other parts of the device, such as the contact

pads and traces, were made of metal (Ti/Au). The PDMS-based microfluidic chip was fabricated on a silicon wafer following a previously described soft lithography protocol[39]. The master replica for rapid prototyping of the PDMS microstructure was patterned using negative photoresist (SU-8 50, MicroChem Co., Newton, MA) on a silicon wafer. First, a layer of SU-8 was spin-coated at 4000 rpm. The SU-8 coated wafer was baked and exposed through a photomask containing the desired patterns. After the post-baking treatment, the SU-8 coated wafer was developed leaving master patterns. Liquid PDMS was poured onto the master replica and cured. And then peeled off the cured PDMS from the master replica after 24 hours. The fabricated PDMS chip was oxygen plasma treated and bonded with the target substrate in which MEAs were fabricated to form the microfluidic channel (Fig. 2.4b). The diameters of inlet and outlet holes in the microfluidic chip were 2 mm. The microfluidic channel height, width, and length were 40 μm, 250 μm, and 3 cm, respectively. Before cells were injected into the microfluidic channel, the fabricated device was cleaned by 75% ethanol and distilled water, and then sterilized by autoclave. After the autoclaving process, all subsequent procedures were performed in a sterile environment. Poly-D-lysine (PDL) is commonly coated on tissue cultureware to promote surface adhesion to the cell membrane. If the channel was immersed in the PDL solution first, the solution would have hindered at the entrance of the channel due to surface tension[29,32]. Hence, the device was first treated with 95 % ethanol for 5 min, followed by rinsing five times with sterile deionized water. Finally, the inside of the microfluidic channel was coated with a PDL (concentration of 0.1mg/mL) and followed by rinsing five times with sterilized water as well. Actually, it is hard to coat the PDL in the surface of the inside of microfluidic channel.

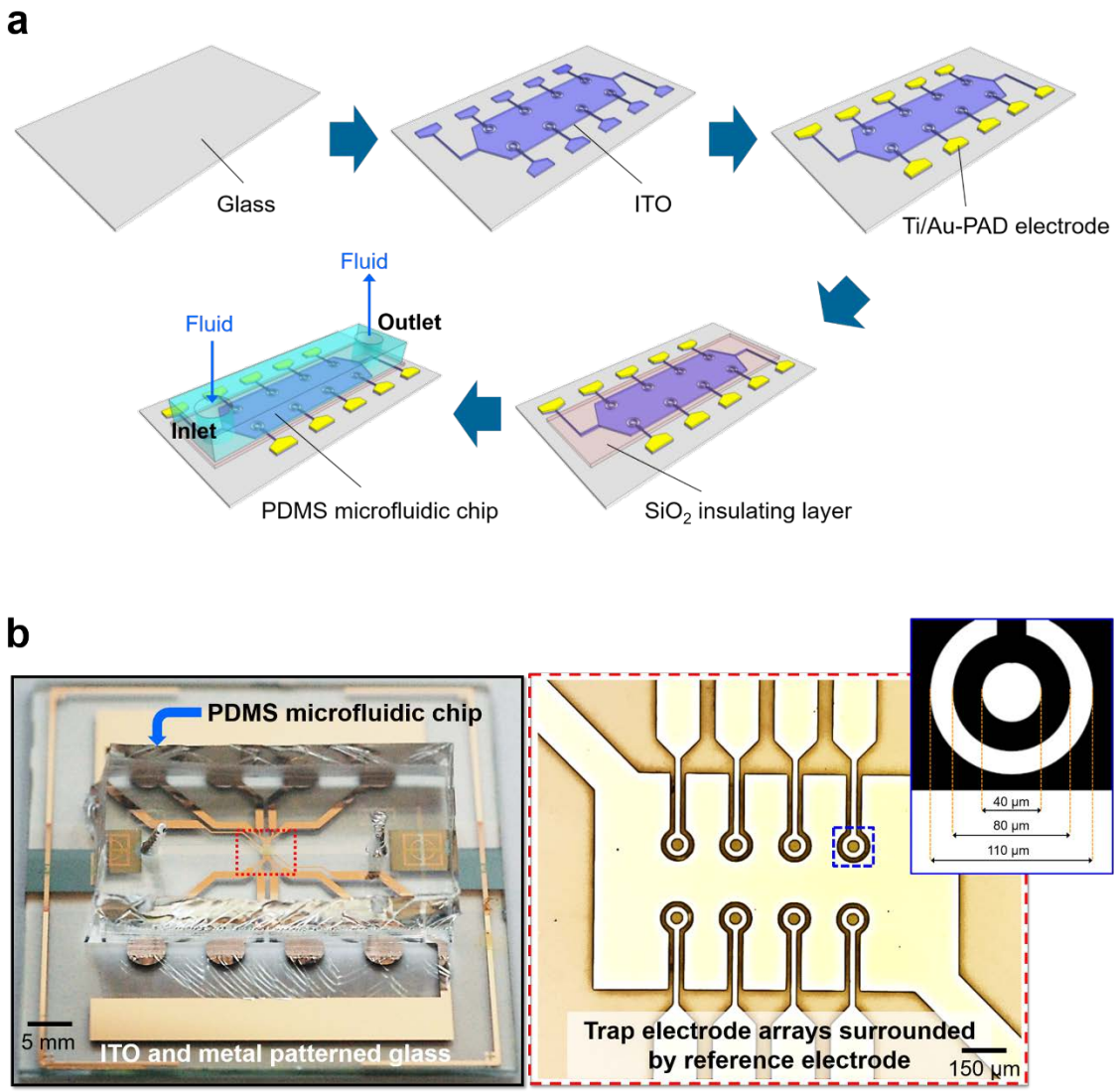

Figure 2.4. Fully transparent microfluidic DEP device. (**a**) Schematic illustration of the fabrication process of the microfluidic DEP device: ITO patterned to form neuron trapping electrodes. Metal patterning of traces and pads on ITO patterned glass. Electrodes are insulated with SiO_2 except metal PADs. Alignment and bonding between electrode patterned substrate and the PDMS microfluidic chip. (**b**) Image of the fabricated microfluidic DEP device and optical microscope image of the electrode arrays. Each ring-

shaped electrode is surrounded by the reference electrode and connected to the metal pads to apply AC signals.

2.4.2 System set-up

The DEP device consists of electrodes arrays patterned on a glass slide and polydimethylsiloxane (PDMS) microfluidic chip fabricated using standard photolithography and soft lithography processes as shown in Fig. 2.4a. The device features a total of eight trap electrodes located in the center of the device with the ability to control each electrode independently to trap and release cells. The use of metal (Ti/Au) pads ensures a stable mechanical connection to the cable connectors used for applying the AC signal. Fig. 2.4b shows an image of the fabricated microfluidic DEP device after the PDMS chip was bonded to the MEAs.

A schematic of the overall experimental set-up for single-neuronal cell trap and culture is depicted in Fig. 2.5a. The fabricated microfluidic DEP device was placed in the incubator that incorporates a motorized inverted microscope (BioStation, Nikon, Inc.). and a CCD digital camera (DS-Qi1, Nikon, Inc.) to facilitate live-cell imaging. A mixture of cell culture media and neurons was loaded onto a 1mL syringe and the needle inserted into the inlet tube (6.25×10^{-2} inch inner diameter) connected to the microfluidic channel designed to flow the mixture. The syringe was placed in a syringe pump (Kent Scientific, Genie plus, CT) set a flow rate of 2.5 μL/min. The AC signal used to trap cells on the electrodes was generated by a function generator (HP 33120A) and its amplitude and frequency were 8 V_{pp} and 10MHz, respectively. In order to prevent signal attenuation, AC signal was applied to the electrode via RF coaxial cable connectors (Taoglas Limited

CAB.058 semi-rigid SMA RF connector), by which impedance was matched to 50 ohms, and was confirmed by the signal measurement using an oscilloscope (Agilent 54621A). Operation of the microfluidic DEP device is depicted in Fig. 2.5b. When the target neuron

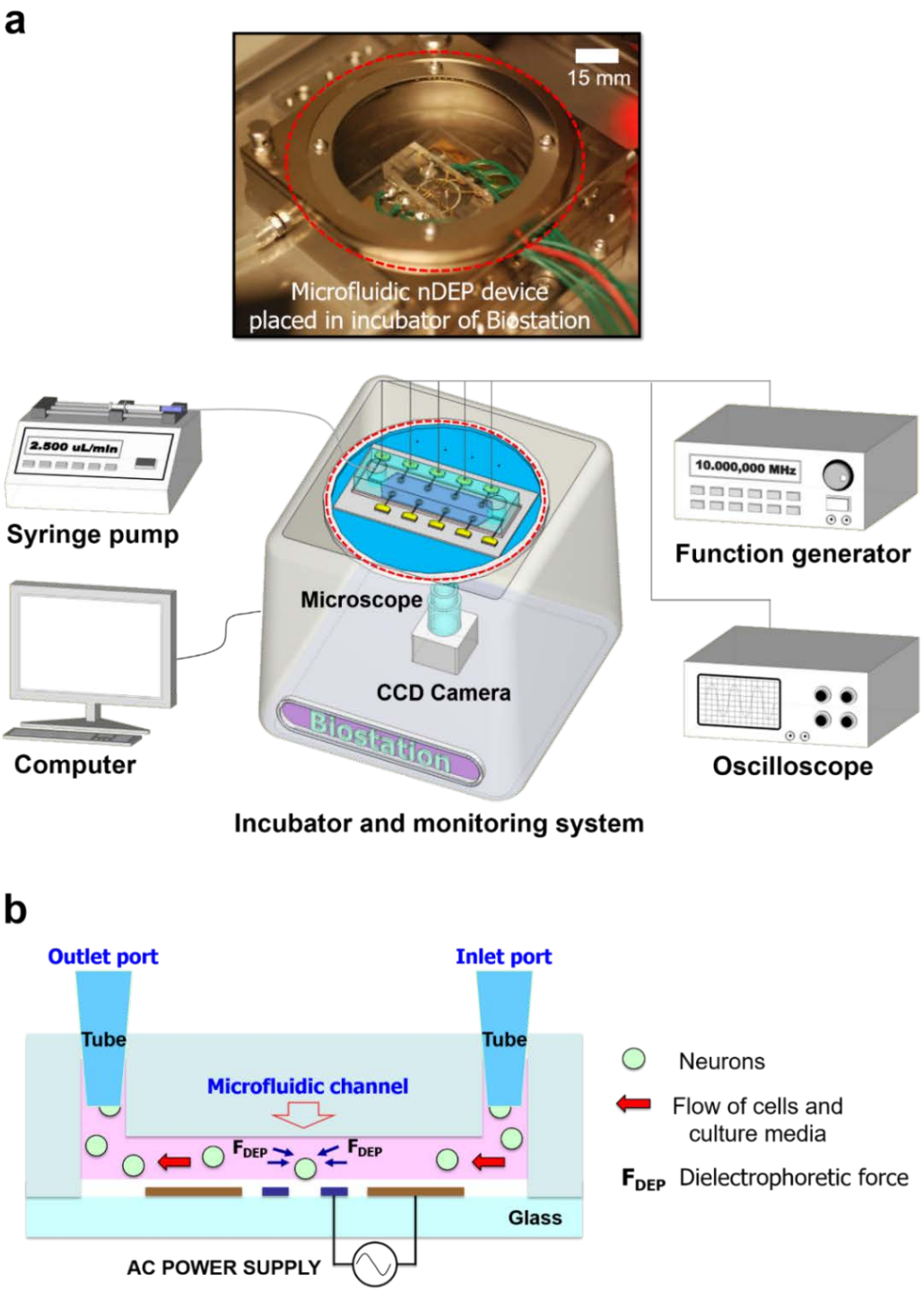

Figure 2.5. Single-neuronal cell trapping and culture system. (**a**) Overview of the cell incubator and monitoring system, as well as an image of the microfluidic DEP device placed in the incubator. The set-up is composed of a syringe pump, a function generator, an oscilloscope, a camera, a microscope and a monitoring computer. Each metal pad of the eight ring-shaped electrodes is connected to the positive terminal of the function generator and the two reference electrodes are connected to the ground terminal of the function generator. (**b**) Schematic illustration of the cross-section of the microfluidic DEP device.

approaches the trap, the electrode is energized to immobilize the neuron at the center of the electrode. After neurons are positioned inside the electrodes, a medium without neurons was introduced into the microfluidic channel to remove the excess cells. Neurons attached to the target electrodes after the medium stopped flowing. The immobilized neurons were cultured and the growth of the neurons was recorded in the incubator.

2.4.3 Cortical neuron culture

All animal procedures were approved by the University of Wisconsin Institutional Animal Care and Use Committee (IACUC) and were in accordance with National Institutes of Health guidelines. Embryonic day (E) 18 cortical/hippocampal neuron cultures were prepared from Sprague-Dawley rats of either sex (Envigo) as described previously[40]. Briefly, cortices were dissected, trypsinized and dissociated. Dissociated cortical neurons were plated on 1.0 mg/mL poly-D-lysine (PDL) (Sigma-Aldrich)-coated DEP device. Neurons were plated in plating media (PM) (Neurobasal medium with 5% FBS (Hyclone),

B27 supplement, 2 mM glutamine, 37.5 mM NaCl and 0.3% glucose). After 1 h, the medium was replaced with serum-free medium (SFM), which was PM without FBS. Neurons were then fixed and imaged after 5DIV.

2.4.4 Immunocytochemistry and imaging

For wide-field imaging, neurons were fixed in 4% paraformaldehyde/Krebs/Sucrose at 37°C. Cultures were rinsed three times with phosphate buffered saline (PBS) solution and blocked with 10% BSA/PBS, permeabilized in 0.2% Triton X-100/PBS and labelled with primary and secondary antibodies. Primary antibodies to the α-tubulin, specifically, Tyrosinated-Tubulin (Millipore) and Tau-1 (Chemicon) and secondary antibodies to goat anti-rat and goat anti-mouse IgG Alexa Fluor 488, 568 and 647 (Invitrogen) were used to visualize microtubules. Phalloidin coupled to Alexa 488, 568 or 647 (Invitrogen) was used to label actin filaments (1:25 to 1:100). Neurons were imaged on a Nikon TE300 inverted microscope equipped with a 40X/1.3NA Plan Apo (DIC-fluor) and 20X/0.5NA (phase-fluor) objective. Images were captured on a Coolsnap EZ cooled interline CCD camera (Photometrics).

2.5 Results

2.5.1 Device modeling and simulation

To verify the feasibility of the proposed DEP device for single neuronal cell manipulation, the strength of the electrical field and the direction of the DEP force over the device including electrodes were numerically solved using finite element simulation software (Comsol Multiphysics 4.2, Comsol Ltd). The amplitude and frequency of the applied

voltage in this simulation were 8 V_{pp} and 10 MHz, respectively. For the designed ring-shaped electrodes, we presumed the electric field distribution to be cylindrically symmetric in any plane orthogonal to the plane of the array of electrodes.

For the simulation, various physical parameters of the structure and a dipolar model of the DEP force were established. The parameters of the neuronal cell and medium were as follows: the radius of the cell: 5 μm, permittivity of the cell: 80, cytoplasm permittivity: 7.1×10^{-10} F/m, cytoplasm conductivity: 0.75 S/m, membrane permittivity: 1.8×10^{-12} F/m, membrane conductivity: 1×10^{-7} S/m and medium permittivity: 7.1×10^{-10} F/m[24,30,35,41,42]. As for the boundary conditions, applied AC electric potentials were on the ring-shaped electrodes and the outer surfaces were set to electrical insulation.

Figure 2.6a shows the distribution of the electric field magnitude (E^2) for each trap electrode with an applied signal of 8 Vpp at 10 MHz. As can be seen in this figure, the magnitude of the electric field changed over the position (x-axis), with a minimum in the center of the ring-shaped trap electrode and maximum at the edge of electrode in the gap between the trap electrode and surrounding counter electrode. Dielectrophoretic forces (white arrows) are directed toward the center of the ring-shaped electrode and repellent forces are displayed near the surrounding electrodes. This simulation result indicates that invisible trap formed at the center of the electrode with low electric field magnitude.

The numerical simulation results of the neuron motion tracking at each instant are illustrated in Fig. 2.6b. Neurons were modeled as blue particles with a radius of 5 μm and distributed uniformly at the initial stage (I) of the simulation. The blue particles placed near the ring trap were driven toward regions of low field strength and collected in the center of the ring trap. However, the particles placed outside of the ring trap moved upwards,

repelled by the repulsive force over time. This simulation indicates that our microfluidic DEP device is suitable for single cell manipulation.

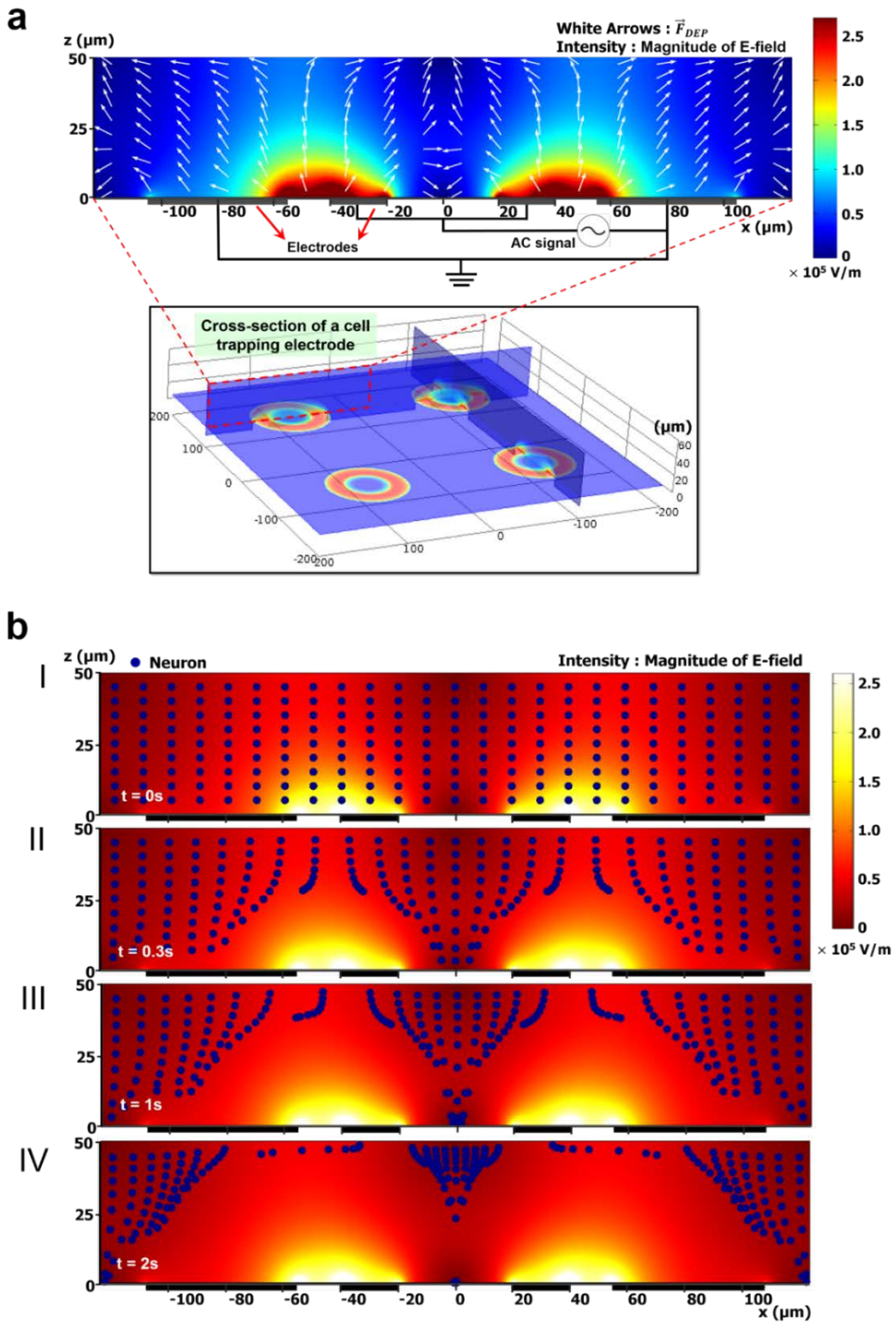

Figure 2.6. Schematic illustrations of trap electrode arrays and its cross-sectional view with numerical simulation results. The color bar shows the electric field intensity (in V/m) for an applied AC signal. (**a**) Distribution of the electric field magnitude (in V/m), based on an applied potential of 8 Vpp at 10 MHz, is shown for each trap electrode inside the fluidic channel with color-scale plot. The white arrows, normalized vectors, indicate the direction of the dielectrophoretic force. The intensity of the applied electric field is maximal in close proximity to the edge of each ring-shaped electrode and is reduced to its minimum value at the center of the trap zone. (**b**) Motion trajectories of neurons with a radius of 5 μm under the distribution of applied electric field magnitude (in V/m). Numerals I-IV correspond to time: (I) Initial distribution of neurons in the domain, (II) position of the neurons after 0.3 s, (III) 1 s, and (IV) 2 s.

2.5.2 Single-neuronal cell manipulation

To demonstrate the performance of our proposed fully-transparent microfluidic DEP device, single-neuronal cell manipulation was conducted as shown in Fig. 2.7. The cell trapping process was carried out inside an incubator and monitored with a built-in CCD camera (DS-Qi1, Nikon, Inc.).

The single-neuronal cell trapping process is illustrated in Fig. 2.7a. The neuronal cells were trapped and released sequentially by an array of ring electrodes arranged in a row. Details of the neuronal cell positioning process are as follows: (I) A target neuron (red arrowhead) flows to the 1st electrode. (II) When the target neuron comes in proximity to the 1st electrode, the 1st electrode is energized and the neuron is immobilized in the center

of the 1st trap site. (III) Non-cellular particles (blue arrowhead) are repelled by the 1st electrode and keep flowing while the trapped neuron remains at the 1st trap site (green arrows). (IV) The trapped neuron is released by turning the 1st electrode off, travels with the flow of the media, and then is trapped again in the center of the 2nd trap site. (V-VI) The neuron is then subsequently released and trapped in turn by the 3rd and 4th trap sites. We also observed neurons being repelled from the electrode. The images in Fig. 2.7b show the bouncing motion of the neuron which is subject to a repulsive force induced by the nDEP. (I and II) While the target neuron was immobilized in the ring trap (red arrowhead), another neuron comes in close proximity to the ring trap and it appears to have bounced off the invisible wall created by the repulsive force (black arrow). (III) The repelled neuron travelled along the invisible wall carried by the flowing media, while the target neuron stays in the trap. The trapping and bouncing motion of the neuron was in concordance with the particle trajectory simulation results (Fig. 2.6b).

2.5.3 Single-neuronal cell culture, monitoring and imaging

After the cell trapping process, the media was aspirated and replaced with fresh culture media to remove any redundant neurons and cellular debris remaining in the microfluidic chamber and deliver nutrients to the trapped neurons. The fluid flow was shut down and the system was stabilized for 5 min. Then, the nDEP forces were turned off so that the trapped neurons levitating above the electrode plane were released from its levitated position and plated down for culture. During the cell culture period, we changed the culture media once a day to supply nutrients to the neurons by aspirating away approximately half of the media and replacing the amount removed with fresh media. The

cultivation images were recorded by a CCD camera integrated inside the incubator. Red LED illumination was used for phase contrast imaging.

To confirm whether the trapped single neurons settle and grow well on the trap electrode, we monitored the morphological changes of growing neurons for 20 hrs. Figure 2.8a shows the time-lapse phase contrast images of neurite outgrowth in an *in vitro* culture of a trapped single neuron. As can be seen in this figure, the morphology of neuron changed slightly after 1 hr and minor neurites began to form after 2 hrs.

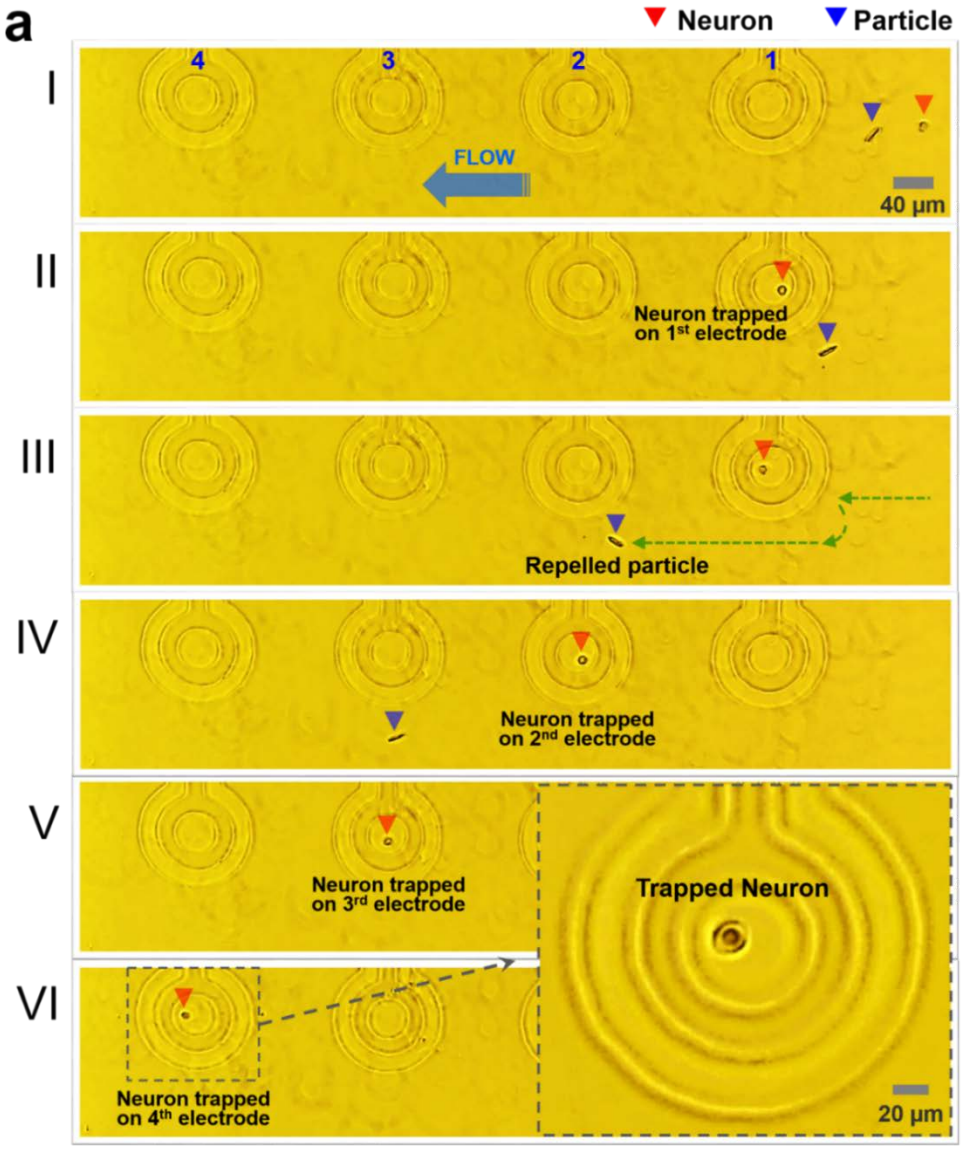

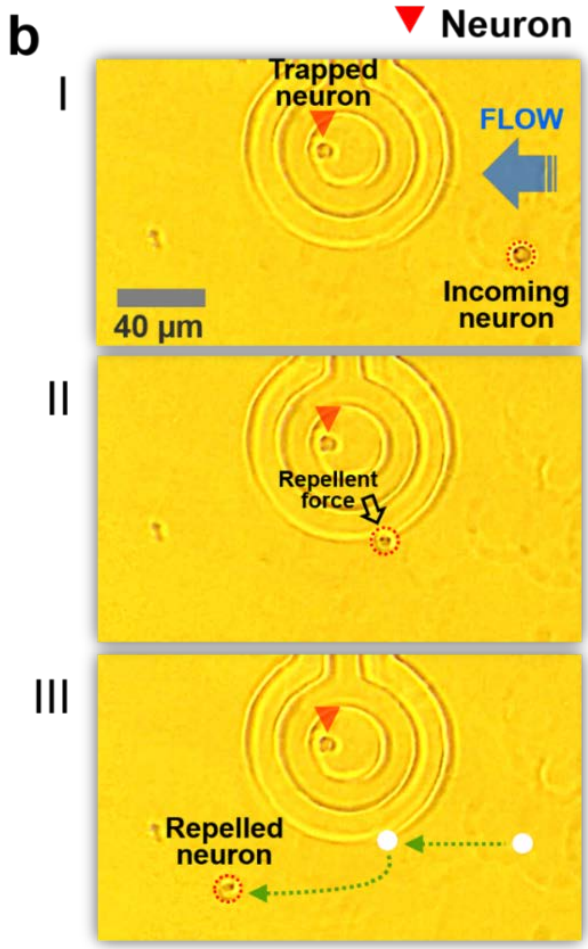

Figure 2.7. Recorded images of single-neuronal cell manipulation on the array of ring-shaped traps. (**a**) Incoming neuron (I) entering the 1st trap. (II) The neuron is then immobilized in the 1st trap electrode against a fluid flow. (III) While the neuron is trapped, a repelled particle continues to move in the flow of media. (IV) The released neuron is captured again in the 2nd trap. (V and VI) The neuron is trapped in the 3rd and the 4th ring trap in turn. (**b**) Bouncing motion of the neuron subject to a repulsive force. While the target neuron was trapped in the desired electrode, an incoming neuron was repelled by DEP force. When the incoming neuron reached the outside of the electrode, the repulsive force pushed the neuron out of the ring.

After 4 hrs, we observed that several minor neurites protruded the cell body and continued to extend over time. These results demonstrate the viability of the technique as we confirmed that a single neuron successfully adhered to the trap electrode and grew well over time.

All of the neurons cultured on the fabricated devices show the same developmental trajectory. First, neurons exhibited a stereotypical series of events in which they first attach to a substrate and extend both lamellipodia and filopodia (stage 1). Over time, filopodia merge and form several distinct neurites, all of which contain a growth cone at their tip (stage 2). Within 48 hours of plating, one of the neurites elongates rapidly to form an axon (stage 3), while the remaining neurites develop slowly into dendrites (stage 4)[43]. A DIC and a fluorescent image of a single neuron cultured on the trap electrode are shown in Fig. 2.8b. Neurons cultured on PDL-coated DEP devices were fixed at 5 days *in vitro* (5DIV) and labelled for microtubules (red) and actin (green). Phalloidin staining at the tips of both neurites and growth cones show typical stage 2 to 3 development, as well as prominent tyrosinated tubulin staining, which labels dynamic microtubules, in both dendrites and axons[44].

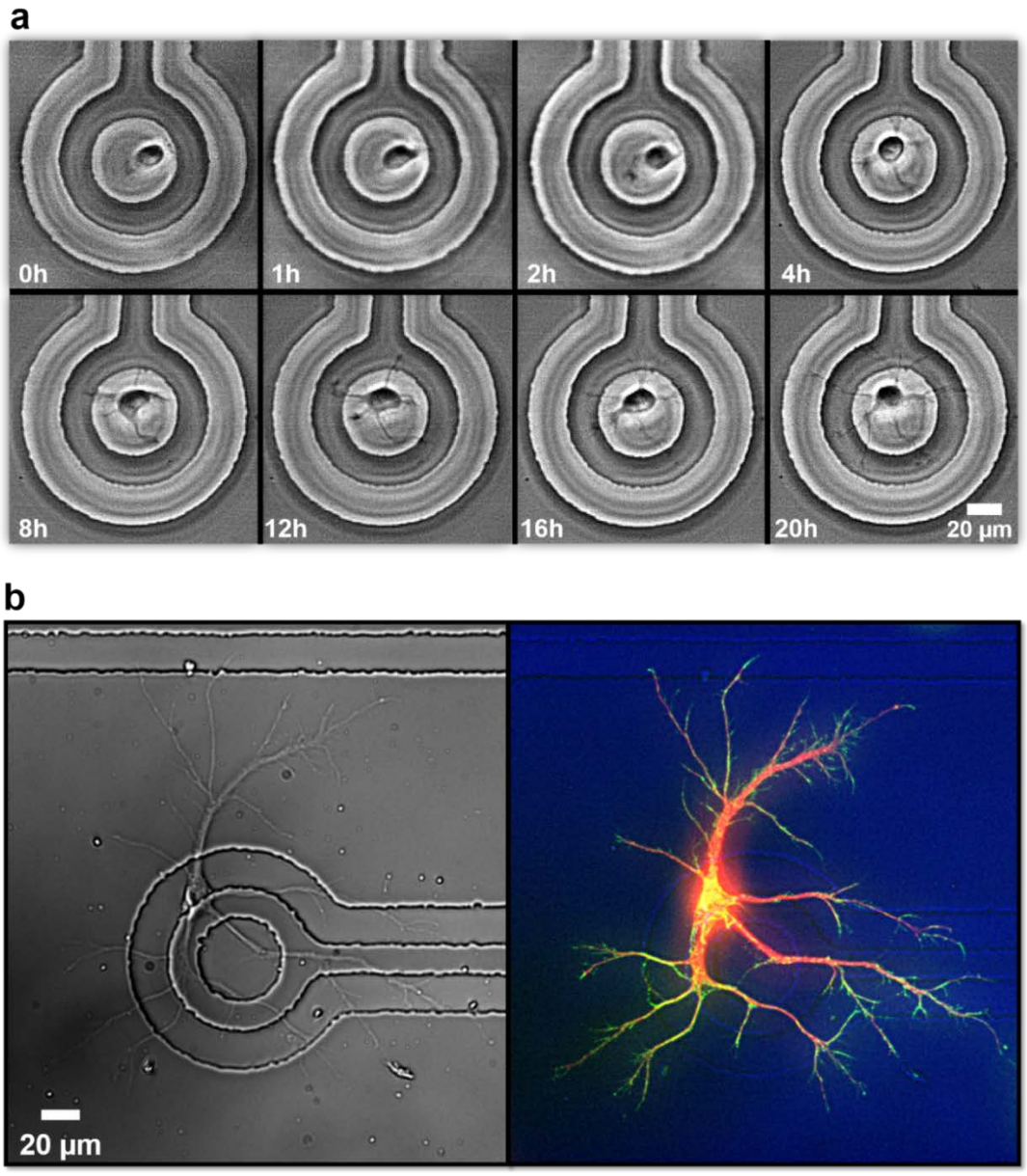

Figure 2.8. Images of cultured neurons on trap electrodes. (**a**) *In vitro* time-lapse imaging of outgrowth of a single neuron on the trap electrode for 20 h. The trapped neuron was attached on the surface at the initial stage of the imaging. Time-lapse phase contrast images of a living cortical neuron show outgrowth of neurites. (**b**) Microscope image of a cultured neuron on a trap electrode (left). Neuron was fixed at 5 days *in vitro* (5DIV). Image of neuron immunolabeled for microtubules (red) and actin (green) (right).

2.6 Conclusion

We have presented an advanced single-neuronal cell culture and monitoring platform which enables single-neurons to be positioned at a desired location. Further, we conducted real-time live-cell imaging within a controlled environment to monitor the outgrowth of neurons while preventing exposure of the neuronal cells to hostile environments. Finite element simulation was used to guide the appropriate design parameters and verify the two-dimensional model of the proposed structures. Following fabrication of the device, we demonstrated the capability to trap individual neurons on specific target electrodes with our DEP device. Changes in cell morphology, such as neurite outgrowth, were accurately observed through the transparent substrate in phase contrast, while avoiding photodamage to neurons that often accompanies fluorescent imaging. Importantly, the applied electric field for DEP did not adversely affect cell health, as demonstrated by live-cell imaging and immunolabelled images as presented in Fig. 2.8a and b. Additionally, the accessibility of neurons appropriately grown on the MEAs makes it possible to record the electrical activity of multiple neurons at the same time, and to investigate the electrical communication between them. Therefore, DEP using MEAs allows not only a label-free and non-destructive technique for cell manipulation but also a non-invasive interface with biological cells for long-term (days to weeks) monitoring of electrophysiological parameters[32,45,46]. Thus, the proposed advanced platform has great potential to form an *in vitro* ordered neuronal network and allows novel and detailed studies of cellular physiology.

2.7 Acknowledgments

This work was supported by Army Research Office (ARO) under grant W911NF-14-1-0652. The program manager is Dr. James Harvey (Dr. Joe X. Qiu, the former). This study was also supported by NIH grant R01-NS080928 to E.W.D.

Chapter 3

The novel combination of cuff and sieve electrodes (CASE) for bi-directional peripheral nerve interfacing

3.1 Abstract

A number of peripheral nerve interfaces for nerve stimulation and recording exist for the purpose of controlling neural prostheses, each with a set of advantages and disadvantages. The ultimate goal of neural prostheses is a seamless bi-directional communication between the peripheral nervous system and the prosthesis. The creation of novel neural interfaces and the surgical methods for their implantation are essential for exploiting the full potential of advanced prosthesis technology required to replace lost limbs. Here, we developed a novel interfacing electrode array, the “cuff and sieve electrodes” (CASE), integrating microfabricated cuff and sieve electrodes to a single unit, to ultimately decrease the weaknesses faced by these electrode designs in isolation. This paper presents the design and fabrication of CASE with *ex vivo* and *in vivo* testing towards chronic application. Electrochemical impedance spectroscopy (Average 820.9±92.9 kΩ at 1kHz), cyclic voltammetry and energy dispersive spectroscopy were performed to determine electrode viability for *in vivo* applications. Finally, terminal device implantations were performed in a rat sciatic transection and repair model to test the ease of implantation and capacity of the CASE interface to write sensory information into the biological system. CASE stimulation of the sciatic nerve at different amplitudes elicited significantly different cortical responses ($p<0.005$) as demonstrated by somatosensory evoked potentials,

recorded via micro-electrocorticography. The ability to elicit cortical responses from sciatic nerve stimulation demonstrates the proof of concept for both the implantation and chronic monitoring of CASE interfaces for innovative prosthetic control.

3.2 Introduction

There are at least 1.6 million people living with limb loss in the United States and an estimated 185,000 new cases occur each year. The number of Americans living with major limb loss is increasing, and expected to double by 2050[7]. Hence, considerable technological efforts have been devoted to develop neural prosthesis devices capable of replacing the motor and sensory functions of lost limbs required to return normative function to amputees[47-50]. With state of the art prostheses now capable of emulating a wide range of limb functions that stand to significantly improve the quality of life of many amputees, the push is now on to develop the ultimate control methods for intuitive control. Peripheral nerve interfaces (PNIs) are one particularly attractive method, offering direct connections between the biological peripheral nervous system and the robotic prostheses.

3.2.1 Peripheral nervous system

The peripheral nervous system (PNS) refers to the parts of the nervous system that are outside the central nervous system, the brain and spinal cord. PNS is constituted by neurons whose cell bodies are located in the spinal cord or within spinal ganglia, their central connections, and their axons, which extend through peripheral nerves to reach target organs. Peripheral nerves contain several types of nerve fibers as shown in Table 2[51]. Afferent sensory fibers terminate at the periphery either as free endings or in specialized sensory

receptors in the skin, the muscle, and deep tissues. Sensory fibers convey various classes of sensory inputs, mainly mechanical, thermal, and noxious stimuli. Efferent motor fibers originate from motoneurons in the spinal cord and end in neuromuscular junctions in skeletal muscles. The majority can be divided into alpha-motor fibers that innervate skeletal extrafusal muscle fibers, and gamma-motor fibers that innervate the spindle muscle fibers. Efferent autonomic nerve fibers in somatic peripheral nerves are unmyelinated postganglionic sympathetic fibers that innervate smooth muscle and glandular targets. Most of the somatic peripheral nerves are mixed, providing motor, sensory, and autonomic innervation to the corresponding projection territory. Nerve fibers, both afferent and efferent, are grouped in fascicles that eventually give origin to branches that innervate distinct targets, muscular, cutaneous, or visceral. Peripheral nerves are organized somatotopically and functionally at the fascicular level. The fascicular architecture changes throughout the length of the nerve, with an increasing number of fascicles of smaller size in distal with respect to proximal segments. Fascicles innervating a given target remain well localized within the nerve for some long distances[52], thus facilitating he selective interface of different fascicles within a common nerve[53]. The Peripheral nerves are composed of three supportive sheaths: epineurium, perineurium, and endoneurium[54]. The epineurium is the outermost layer, composed of loose connective tissue and carries the blood vessels supplying the nerve. The perineurium that surrounds each fascicle in the nerve is composed of inner layers of flat perineurial cells and an outer layer of collagen fibers. The endoneurium is composed of collagen and reticular fibers and an extracellular matrix occupying the space between nerve fibers within the fascicle. The endoneurial collagen fibrils form the walls of the endoneurial tubules, in which axons are accompanied

by Schwann cells, which either myelinate or just surround them. The actions of the body are controlled by neural signals conducted by efferent nerve fibers to activate different muscles. Each spinal motoneuron makes synaptic contacts with a number of muscle fibers, constituting a motor unit. Graded contraction of each muscle is produced by increasing the number of motor units activated and the frequency of impulses to each motor unit.

Table 2. Categories of the PNS

Fiber type	Function	Diameter (m)	Conduction velocity (m/s)
Myelinated			
Aα	Alpha-motor efferents, Proprioceptive afferents	12-22	60-120
Aβ	Tactile, proprioceptive afferents	6-12	40-70
Aγ	Gamma-motor efferents	3-5	30-45
Aδ	Pain, cold afferents	2-5	10-30
B	Preganglionic autonomic efferents	1-5	3-15
Unmyelinated			
C	Postganglionic autonomic efferents	0.3-13	0.7-2.3
C	Thermal, pain, mechanical afferents	0.3-13	0.5-2.0

Recruitment of motor units follows a size-dependent order, with slow fatigueresistant motor units activated first and large fast fatigue motor units activated only at high levels of tension. On the other hand, the information transduced by the natural receptors is conducted to the CNS by the afferent nerve fibers. Each somatic sensory neuron is specified to a

sensory modality, touch, proprioception, temperature, or pain, depending upon the specialized terminal receptor. Each sensory neurons subsides a receptive field in the peripheral tissue, of variable size according to the body segment. Signals are transmitted by the corresponding axons in series of action potentials, with intensity of the signal mainly coded by impulse frequency.

3.2.2 Peripheral nerve electrodes

PNIs normally detect the bioelectrical activity of the nerve fibers using coupling method. Hence, most interface electrodes are implanted around or within a peripheral nerve or spinal root to reduce tissue resistance and stimulus intensity. PNIs can be broadly categorized into four general schemes based on levels of invasiveness and selectivity: (1) regenerative, (2) intraneural, (3) intrafascicular, and (4) extraneural, as shown in Fig. 3.1[51]. The selectivity of stimulation or recording individual nerve fibers increases with the invasiveness of the electrode implantation.

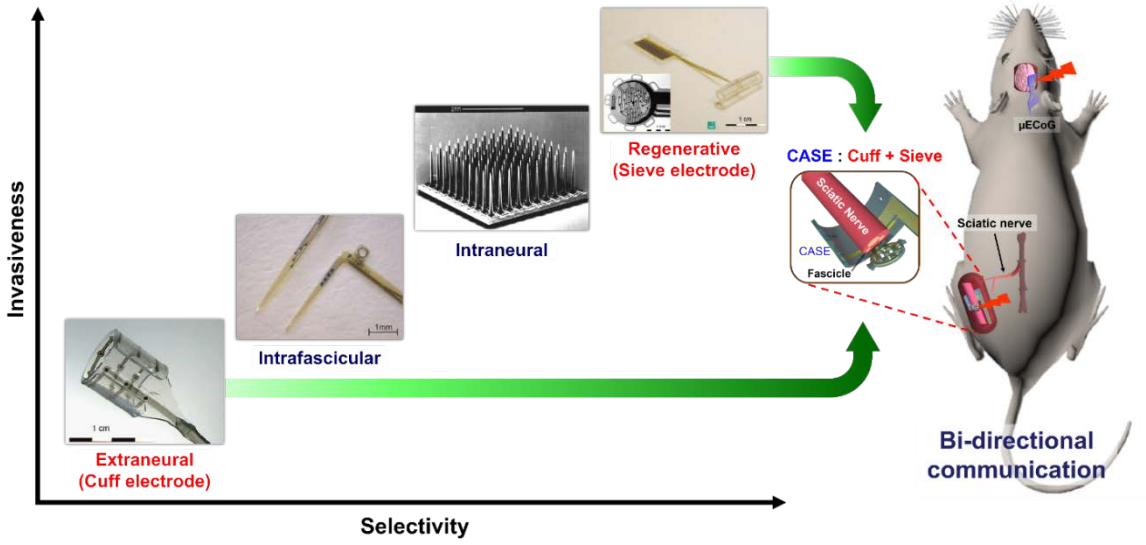

Figure 3.1. Motivation for device development and concepts of CASE implantation. Classification of PNIs are depicted in the image. This represents a broad classification. CASE is designed to integrate the advantages of both regenerative (sieve) and extraneural (cuff) electrodes.

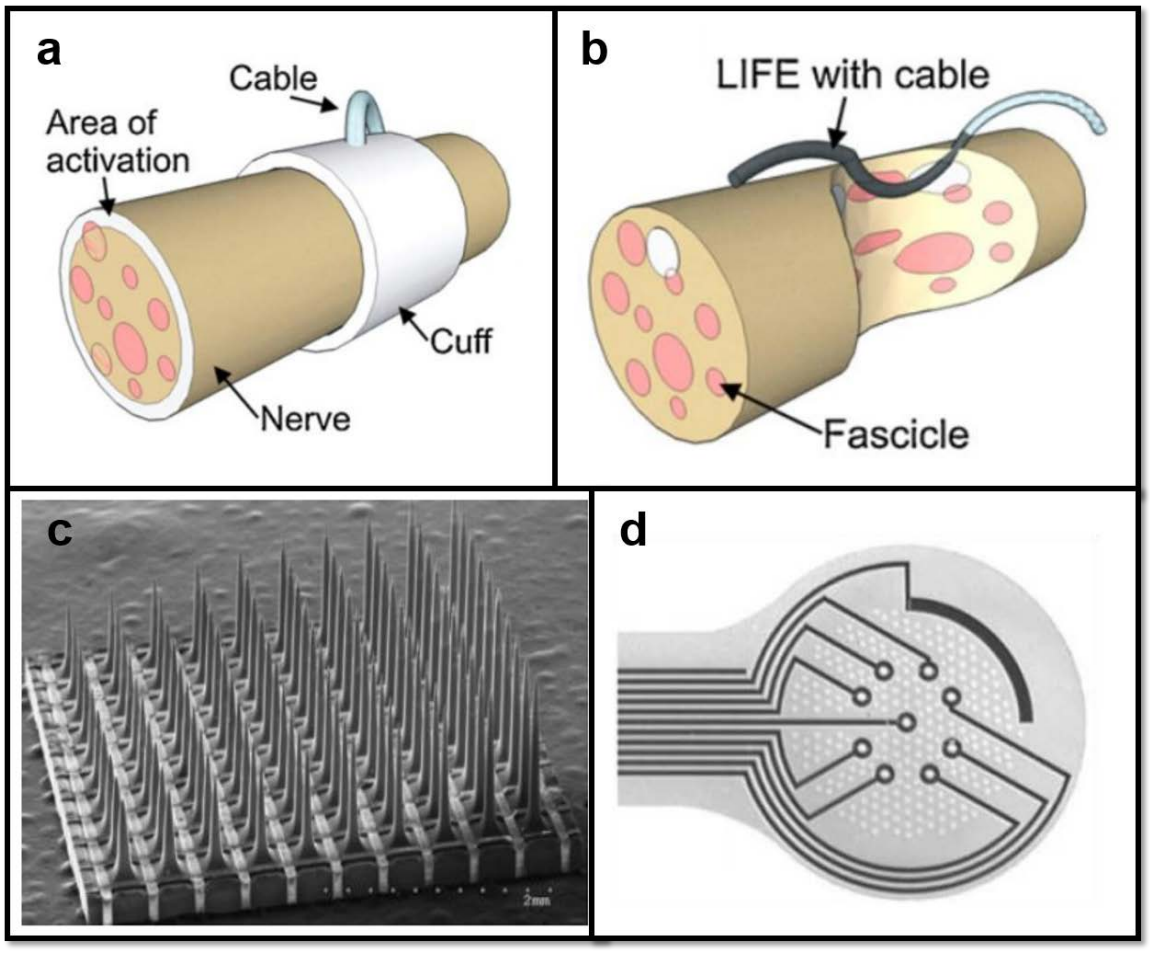

Figure 3.2. Traditional peripheral nerve interfaces. (**a**) Cuff electrode. (**b**) Penetrating Longitudinal Intrafascicular Electrode. (**c**) Penetrating Utah Slanted Electrode Array. (**d**) Regenerative Sieve electrode. Adapted from Boretius, Biosensors and Bioelectronics, 2010; Branner, IEEE Transactions on Biomedical Engineering, 2004; Negredo, Neuroscience, 2004[55-57].

3.2.2.1 Extraneural electrodes (Cuff electrodes)

Extraneural electrodes (cuff electrodes) are regarded as having lowest invasiveness and selectivity. Extraneural electrodes are wrapped around nerves (Fig. 3.2a) and measure electrical potential from the surface of the epineurium. The major caveat to such devices is the lack of recruitment selectivity and the requirement for high current thresholds[58]. Extraneural electrodes are the most widely used electrode in clinical applications for their ease of implantation and robustness, while regenerative electrodes are yet to be tested in clinical application and remain largely experimental. Despite the lack of selectivity cuff electrodes provide, there has been a substantial degree of clinical success in both the motor and sensory control of neural prostheses[59]. Recently, MacEwan *et al.* (2016) demonstrated chronic stable implantation of a novel micro-sieve regenerative electrode in rats, assisted by the use of nerve guidance tubes for stability, such as those commonly used in nerve gap repair[60,61]. Guidance tubes themselves are but a few electrodes away from being an interface of their own, and certainly several novel peripheral interfaces have applied guidance tubes in their design in a tissue engineering approach to peripheral interfacing[62].

3.2.2.2 Intraneural Electrodes (Penetrating Electrodes)

The Longitudinal Intrafascicular Electrode (LIFE) is penetrating interface with a wire like electrode that is inserted longitudinally into the nerve along the direction of the axons (Fig. 3.2b). It also has improved stimulating and recording fidelity and specificity due to proximity of electrodes to axons but currently with only a limited number[63,64]. However, while showing a balance between specificity and reliability[65], the insertion still causes damage to the remaining viable portion of the nerve. Perhaps most importantly, by design

the LIFE is limited to a small number of electrodes when compared to the FINE or USEA and simply does not scale to the level necessary for functional and viable interfaces for amputees. The Utah Slanted Electrode Array (USEA) with 100+ needle-like electrodes (Fig. 3.2c) penetrates into the nerve and resides within individual fascicles, axon bundles. This design provides direct contact between electrodes and axons and leads has demonstrated enhanced specificity over a large number of channels in acute experiments[53,65]. However, the insertion causes irreparable physical damage to the nerve, which would have already undergone significant trauma in the case of limb amputation. Additionally, the USEA electrodes suffer from chronic inflammation and the eventual formation of scar tissue and fibrotic encapsulation. Due to these drawbacks, the overall efficacy has been limited to 80% of the electrodes for approximately 5 months in chronic experiments[56].

3.2.2.3 Regenerative Electrodes (Sieve Electrodes)

Regenerative electrodes are designed to contact the transverse face of a severed nerve, allowing axonal growth through the electrodes sites and providing direct and independent access to the distinct fascicular organisation reducing the amount of current required and providing selective spatial recruitment [60,66]. There exists a large trade-off between the ability to selectively interface with individual axons versus the amount of disruption to the nerve and long-term stability as a result of trying to get in close proximity to axons[67]. In order to combat the negative outcomes of trying to get in close proximity to axons, a regenerative approach has been explored where amputated nerves are encouraged to regenerate into specific geometries within close proximity to electrodes. While this

approach is dependent on a previously cut nerve and therefore limited in application, it is advantageous because it allows close proximity between axons and electrodes without the need to penetrate the nerve[68-71]. However, these approaches have met again with limited success. The Sieve Electrode, the hallmark regenerative interface, is effectively a thin perforated disk that is attached to the nerve perpendicularly so the nerve is forced to regenerate through the device[57]. Some of the perforations in the disk have ring electrodes that contact the axons regenerating through the holes (Fig. 3.2d). Theoretically, each hole could have a ring electrode allowing this device to interface with an extraordinarily large number of axons. Designs such as the Sieve Electrode demonstrate highly selective stimulation after regeneration but limited recording fidelity. This is in large part due to the challenges of recording the very low amplitude action potentials (APs) from axons and a spatial dependence of the electrodes to the Nodes of Ranvier where the AP is largest [68,72].

3.2.3 Concept of the proposed novel peripheral nerve interface

Despite the lack of selectivity cuff electrodes provide, there has been a substantial degree of clinical success in both the motor and sensory control of neural prostheses [59]. Recently, MacEwan *et al.* (2016) demonstrated chronic stable implantation of a novel micro-sieve regenerative electrode in rats, assisted by the use of nerve guidance tubes for stability, such as those commonly used in nerve gap repair [60,61]. Guidance tubes themselves are but a few electrodes away from being an interface of their own, and certainly several novel peripheral interfaces have applied guidance tubes in their design in a tissue engineering approach to peripheral interfacing [62].

Here, we present a novel combination of cuff and sieve electrodes (CASE) that integrates the advantages of both regenerative and extraneural electrode for future applications in prosthesis control as shown in Fig. 3.1. The electrode array of CASE is intended to provide ease of implantation and chronic stability while maximizing electrode contacts as well as flexibility in recording/stimulating paradigms through both cuff and sieve portions. As a bi-directional translator of biological and computational signals, CASE can play a pivotal role for harnessing the full potential of advanced prostheses.

3.3 Materials and methods

3.3.1 CASE design and fabrication

We developed a novel design of CASE which combined multichannel sieve electrodes, through which a sciatic nerve regenerates, and cuff electrodes made of a cylindrical sheath which wraps around the exterior of a sciatic nerve. Both the sieve and cuff portions are intended to provide bidirectional neuronal signal communication, independent of each other or in unison. Sieve electrodes provide direct access to the different fascicles that make up the nerve, ultimately providing greater specificity in relation to both sensory and motor signalling required for prosthetic control. CASE was designed to take advantage of the wide range of fascicular topographies that naturally occur in major nerves of the extremities[73,74]. In order to implant sieve electrodes, some form of guidance material is often required to stabilize the device and guide the nerve regeneration through the sieve[60,75,76]. By adding electrode sites to the guidance material, we are able to create an additional cuff electrode that not only improves ease of implantation and stability of the sieve device but also provides additional degrees of functionality. This study focused on

the implantation of the CASE and structural topography of a sciatic nerve; which is a mixed sensory-motor nerve, utilizing the additional cuff electrode as the return path. CASE were manufactured by a sandwich structure using flexible and biocompatible material, parylene-metal-parylene, with exposed electrode sites and pads[77]. The number and size of electrodes can vary according to the desired application. The detailed design of combined cuff and sieve electrode (CASE) is depicted in Fig. 3.3a. Eight ring electrode sites spread out uniformly to form the sieve portion of the device to make independent contact with the varying fascicular topography and two rectangular electrode sites placed across the cuff portion of the device to make epineural contact when CASE wrapped around the nerve. We designed additional square shaped parylene wings with holes on both sides of sieve face to allow easy suture placement when securing the sieve face to the epineurium, ultimately forming the interface. Each sieve and cuff electrode is connected to an insulated lead wire. Two cuff electrode sites are formed on the body part and can be used for grounding or return path for the applied signal as well. In addition, CASE was designed to be installed on a peripheral nerve with the use of securing sutures. Five pass-through suturing holes were included in the body to adjust the size of the cylindrical sheath of the device. The specifications of the electrodes, pads, traces and holes are as follows and depicted in Fig. 3a as well: inner and outer diameter of the sieve electrode, 160 μm, 380 μm, respectively; width of the sieve electrode, 50 μm; diameter of the penetrating holes, 60 μm; cuff electrode width, 150 μm; cuff electrode length, 1500 μm; diameter of suturing hole, 300 μm; width of body part of CASE, 7300 μm; and length of CASE, 11.5 mm.

Platinum-based electrode arrays were fabricated on Parylene C coated wafers as illustrated in Fig. 3.3b. The details of the fabrication process can be found in the

experimental section and our previous paper as well[77,78]. Briefly, metal electrode arrays were fabricated on a Parylene C coated silicon wafer. Electrode sites, connecting traces and pads are made of stacked titanium (Ti), gold (Au), and platinum (Pt) metals. To increase the surface area of the electrode and reduce electrode impedance, platinum gray was electroplated on the exposed electrodes [79]. The fabricated electrodes were inserted in a zero insertion force (ZIF) connector on a printed circuit board (PCB) (Imagineering Inc., Elk Grove Village, Illinois) to connect the device to a potentiostat and an electrical stimulator.

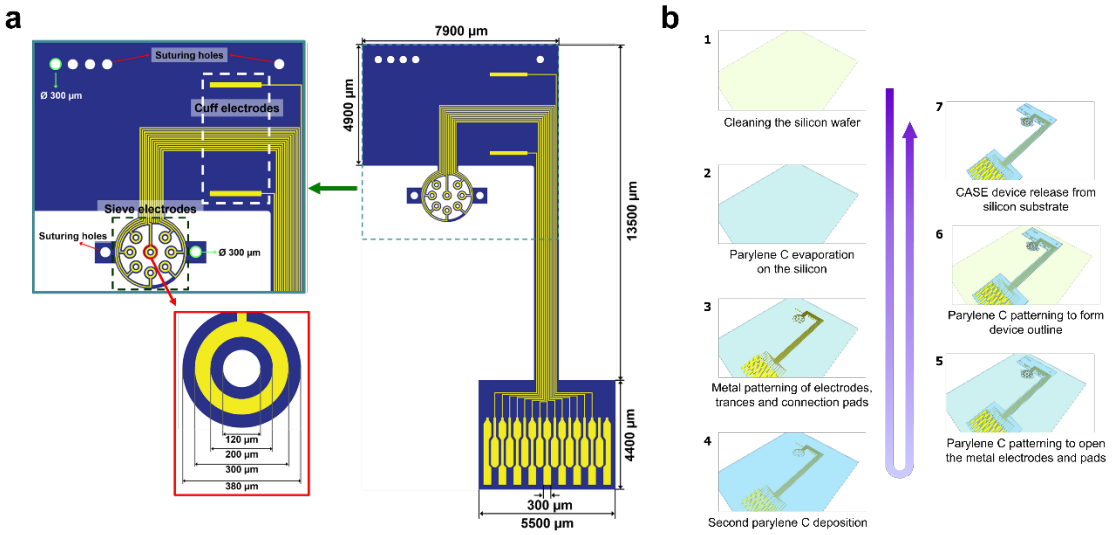

Figure 3.3. Design of CASE and manufacturing process. (**a**) Detailed design of CASE including measurements of relevant features. (**b**) Fabrication process: metal patterning of electrodes, traces and connection pads on Parylene C/silicon wafer. After metal patterning, second parylene C was deposited and patterned form device outline. Removal of device from silicon wafer.

3.3.2 Electrochemical impedance spectroscopy (EIS), Cyclic voltammetry (CV)

A three electrode system was used for the measurement. The arrayed CASE electrode served as the working electrode (WE), a coiled Pt electrode as the counter electrode (CE), a Ag/AgCl electrode as the reference electrode (RE), and phosphate-buffered saline (PBS, pH 7.4, 0.1M) as an electrolyte solution at room temperature. The 8-channel CASE device was connected to the Autolab PGSTAT 128N (Metrohm Autolab, Netherlands) *via* a zero insertion force (ZIF) printed circuit board (PCB). For the EIS, 10 mV sine waves at frequencies from 1 to 100 kHz were used and the parameters of the equivalent circuit were extracted using Nova 1.10 software (Metrohm Autolab). CV scans were taken from -0.6 to 0.8 V with a step potential of 10 mV and a scan rate of 50 mVs^{-1}. The details of this measurement set-up can be found in our previous papers [77,78,80]

3.3.3 Scanning electron microscopy (SEM) & Energy Dispersive Spectroscopy (EDS)

The surface features of the electroplated Pt electrode were characterized using field emission scanning electron microscopy (FE-SEM, JEOL, JSM-6701F, Japan) at accelerating voltage of 10kV with 50,000 magnitudes. And we coated the surface of specimen with 30 nm of thickness Au. And a typical EDS spectrum allows one to identify what those particular elements are and their relative proportions (Atomic weight% for selective area). X-ray spectrum was generated from the selective area. The Y-axis shows the counts (number of X- rays received by the detector) and the X-axis shows the energy level of those counts.

3.3.4 *In vivo* acute stimulation and recording setup

Sciatic nerve stimulation was achieved using the sieve portion of CASE, utilizing independent electrodes (Fig. 3.4a) to stimulate different areas of the sciatic nerve, while the cuff electrode was utilized as the return path. All data was recorded from somatosensory cortex via a µECoG placed over the contralateral cortex relating to the interfaced hind limb. Both CASE and µECoG were connected to a TDT system via zero insertion force (ZIF-Clip) Clip Digital Headstage (Tucker-Davis Technologies, Florida, USA). Ground and reference wires for both the CASE and µECoG were placed in surrounding musculature. Bipolar stimulation of the CASE electrode was performed via a TDT IZ2H stimulator controlled by the TDT RZ5 BioAmp Processor. Stimulation was a charge balanced single biphasic pulse with 200 µs phase and an amplitude ranging from 100 µA to 500 µA. A cathodic leading stimulus was applied to a single channel within the sieve portion of CASE. The most proximal pad electrode of the cuff was used as the return path for stimulus. Cortical responses evoked by stimulation were amplified (2x), bandpass filtered (corner frequencies: 2.2Hz – 2.7kHz) and digitized at 6kHz using a PZ5 NeuroDigitizer (Tucker-Davis Technologies). Approximately 20 minutes before the start of stimulation, anesthesia was switched from isoflurane to a ketamine (25-100mg/kg) and dexmedetomidine (0.05-0.1mg) cocktail as isoflurane is known to reduce cortical activity.

3.4 Results

3.4.1 Fabricated device characterization

The manufactured CASE is shown in Fig. 3.4a. Anchoring holes for suturing and central sieve holes for nerve regeneration were fully etched out (Fig. 3.4b). All traces were

connected to the pads formed on the parylene for connection to the ZIF PCB (Fig. 3.4a). Traces were covered with parylene, but the pads needed to be opened. And a microECoG (μECoG) was also fabricated for data recording from somatosensory cortex. The detailed fabrication process and characterization of the μECoG were described well in our previous papers [77,78,80-82]. Electrochemical impedance spectroscopy (EIS) and cyclic voltammetry (CV) are fundamental tools used to estimate the abilities of the CASE for recording and stimulation[83]. To increase the surface area of the electrode and reduce electrode impedance, platinum was electrochemically deposited to microelectrodes on CASE[79]. SEM image of electroplated platinum microelectrode is shown in Fig. 3.4e. The porous surface morphology was observed by SEM imaging. Energy dispersive spectroscopy (EDS) analysis results for the electroplated surface are shown in Fig. 3.4f. Main elements, Au (72.22wt%), Pt (9.16wt%) and Ti (0.97wt%) are the most abundant in the selected field. Impedance spectra were obtained for electrode sites *in vitro* using an Autolab PGSTAT 12 potentiostat with 3 electrodes tested in the frequency range from 1 to 100 kHz. We measured the electrochemical impedance of each electrode at 1kHz, the benchmark frequency of neural electrodes [84,85]. The details of measurement setup described in our previous papers as well [77,78]. Representative EIS measurement results for CASE are shown in Fig. 3.4g and h. The average impedance of channels was 280.9±92.9 kΩ for electrodes with an area of 39,270 μm^2. The phase was over a 75° at 1 kHz, presenting a mainly capacitive charge transfer mechanism. This is an ideal property for neural stimulation as no chemical change occurs to either the tissue or the electrode. In addition to EIS, cyclic voltammetry (CV) was also performed on CASE devices using the Autolab system. CV scans were taken from -0.6 to 0.8 V with a step potential of 10 mV and a scan rate of 50

mVs^{-1}. The voltage range was chosen in order to stay within the water window. Average CV curves for CASE devices are shown in Fig. 3.4i. Except for a small peak at -0.2 V, most likely due to the reduction of oxygen, the CV plot shows no faradic reactions.

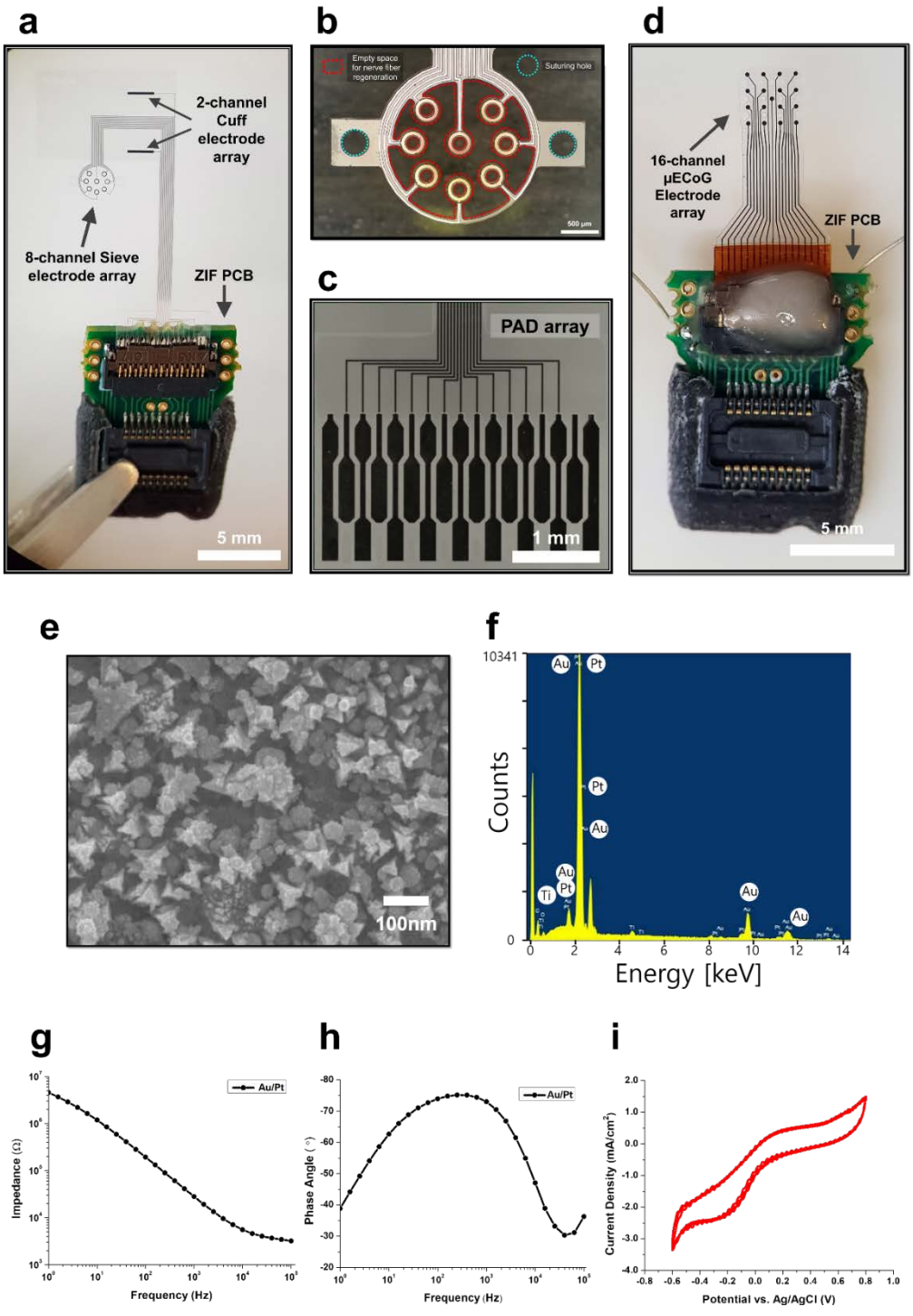

Figure 3.4. Fabricated CASE electrodes and their characterizations. (**a**) CASE device with 8 sieve and 2 cuff electrode sites. CASE is inserted into a ZIF PCB connector. (**b**) Sieve portion of the CASE. (**c**) Pads for connection to the zero insertion force (ZIF) printed circuit board (PCB). (**d**) µECoG array with 16 electrode sites and a ZIF PCB connector. (**e**) SEM images of the electroplated Pt-gray on the electrode. (**f**) Energy Dispersive X-ray Spectroscopy (EDS) analysis result. The results of (**g**) electrochemical impedance spectroscopy (EIS) for impedance and (**h**) phase angle. (**i**) Average cyclic voltammetry (CV) results for 8 electrode sites.

3.4.2 Surgical procedure for CASE Implantation

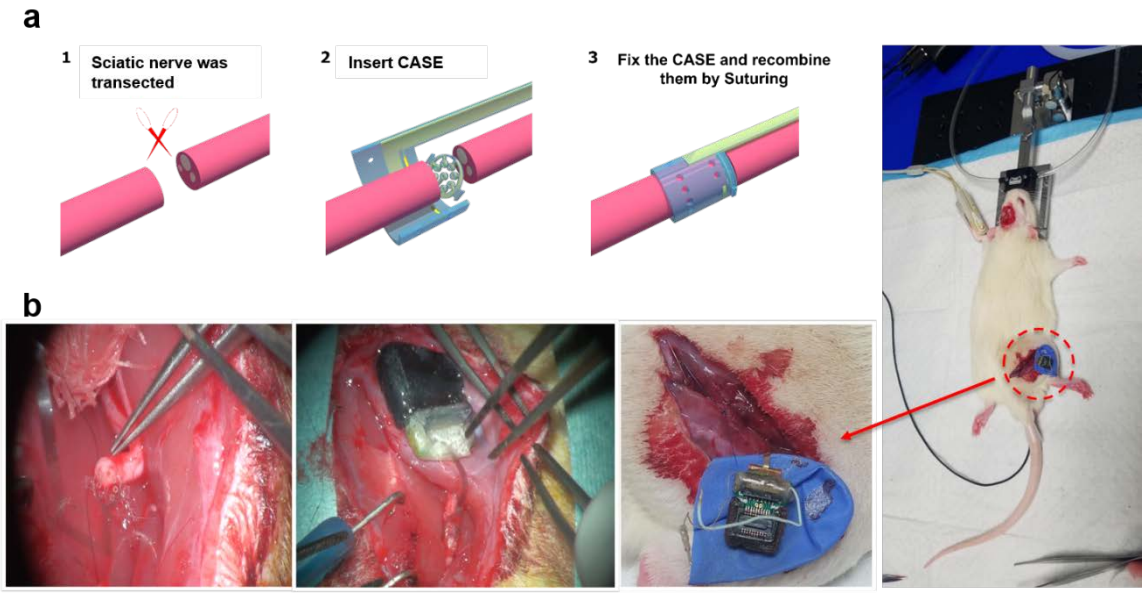

Figure 3.5. Rat surgery and device implantation procedure. (**a**) illustration of CASE implantation procedure. (**b**) Implanted CASE on rat.

Terminal implantations were performed on rats and the implantation procedure is outlined in Fig. 3.5a (steps 1-3). All animal procedures were approved by the Institutional Animal

Care and Use Committee at the University of Wisconsin-Madison and conformed to US National Institutes of Health guidelines. Terminal implantations were performed on male Lewis rats, aged 4-6 months (n=4). Procedures were conducted utilizing aseptic techniques despite their acute nature. Animals were anesthetized with 5% (induction), and 2% (maintenance) inhaled isoflurane. Animals was placed prone in a sterotax for head imobilization and the hindlimb was abducted with the knee flexed, and the ankle taped to the operating table. Following shaving, a line was drawn along the palpated femur and a longitudinal posterolateral thigh incision was made 2-4 mm posterior to this line. The biceps femoris was divided, reflected caudally, and the sciatic nerve visualized. Microdissection to free the sciatic nerve proceeded circumferentially and proximally until fascicular branches of the sciatic nerve could not be identified by epineural inspection. A thread of gauze was gently wrapped around the circumference of the nerve and compared to the CASE to determine correctly spaced suturing holes (Fig. 3.5b). The CASE, connected to a ZIF PCB, was inserted beneath the nerve with the neck of the sieve ring underlying the desired transection point. The nerve was then transacted using straight microscissors. The proximal and distal ends were then sutured together using two epineural stiches, with each passing through one of two sieve insertion tab holes at 0 and 180 degrees. During this process, the tightening of the sutures resulted in the upward flexion of the sieve at the neck into the site of transection, establishing fascicular contact. Two additional epineurial stiches were placed at 90 and 270 degrees independent of the sieve. Suture was then passed through two suture holes within the body of the cuff, chosen based on the spacing determined as previously described, and tightened to close the proximal portion of the cuff. Finally, a sling was tied around the cuff near the distal portion utilizing the distal

suture holes for extra support. Finally, a µECoG was placed over somatosensory cortex for recording of somatosensory evoked potentials (SSEPs), as previously described[81,82]. Briefly, a skin incision was made over the calvarium, and soft tissue bluntly dissected to expose cranial sutures bregma and lambda. A craniotomy was performed contralateral to the transacted and repaired sciatic nerve, as close to the coronal and sagital suture lines as possible. The µECoG was then placed on the dura with a stereotaxic electrode positioner.

3.4.3 *In vivo* acute stimulation and recording results

Touch perception is not only an integral component of successful prosthesis control, but also contributes heavily to a sense of embodiment[86]. Sensory perception for prosthesis use remains one of the major confounding factors to achieving elegant prosthetic control as well as acceptance of a prosthesis as a part of oneself, and is therefore the focus of the proceeding experiments. The potential for CASE to serve as a viable PNI was examined *in vivo* using an acute implantation model, demonstrating the ability to write sensory information to the brain via the CASE interface. Stimulation of the sciatic nerve with CASE was performed across a range of amplitudes through two independent electrodes located on opposite sides of sieve portion, the resulting responses were recorded cortically as somatosensory evoked potentials (SSEPs) via µECoG demonstrating statistically significant responses based on amplitude and electrode position ($p=<0.005$, Fig. 3.6). The sciatic nerve is a mixed sensory-motor nerve with a complex anatomical topography that we aimed to access specifically with the sieve portion of the CASE and as such the nature of the terminal experiments focused on the potential to access this rich information source for future chronic studies. As cuff electrodes present a binary stimulation/record paradigm,

this function is more applicable to chronic studies and as such, the cuff electrode was utilized as the return path in these experiments to simply demonstrate the active electrode sites. When the sciatic nerve is stimulated through channel 4 on the sieve face a statistically significant cortical response is not achieved prior to the point of saturation at 400µA ($p=<0.005$, Fig. 3.6). Stimulation of channel 12 however, demonstrates a statistically significant graded cortical response to stimulation amplitude indicating a superior contact with the face of the transacted nerve than channel 4. Heat maps of the SSEP responses highlight that while no spatial differences in cortical response were achieved at the point of implantation this is likely to change as a function of time being that the purpose of these electrodes is to interface with regenerating nerve fibres (Fig. 3.6D-F). These results highlight the importance of surgical approach for neural interfacing as we demonstrate that direct contact with the regenerating nerve front can be achieved at the point of implantation with immediate functional implications. Chronic implantations of CASE interfaces to quantify the impact on regenerated nerves is on-going.

3.5 Conclusion

In summary, we have demonstrated the fabrication of a novel thin-film peripheral nerve interface combining both traditional cuff and sieve electrode (CASE) interfaces with the capacity to act in both an intraneural and extraneural capacity. Generation of somatosensory evoked potentials generated through the CASE viability of electrical stimulation and bi-directional communication with CASE neural electrodes implanted in rat. Animal experiments incorporating CASE may be carried out over various time scales from hours to years, as long-term recording or behavioural tests may be performed with a

chronically implanted device as shown in Fig. 3.7. Long-term recording with a chronically implanted CASE to quantify the impact on regenerated nerves is on-going. These applications would further validate the use of CASE electrode technology into potential clinical applications. Lastly, the use of this technology with CASE will create a multi-modal platform for investigating the mechanisms of neuromodulation for various neurological disorders.

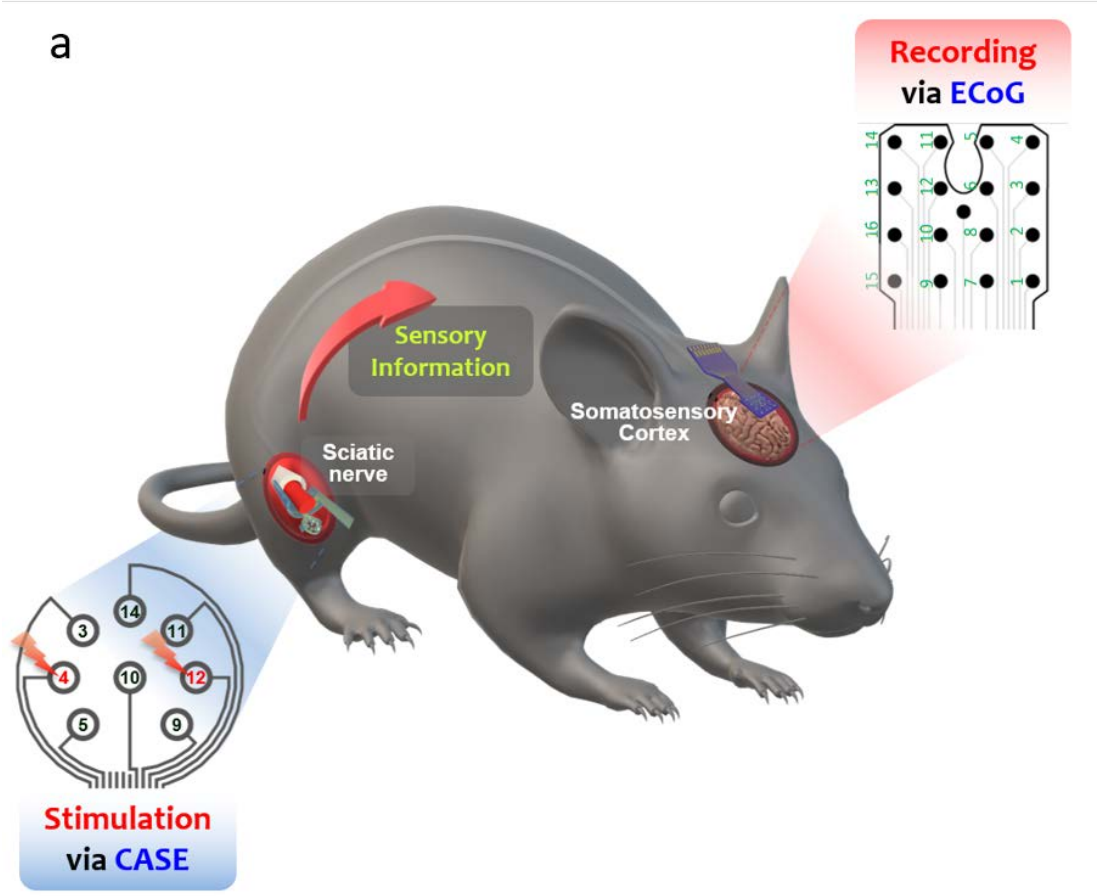

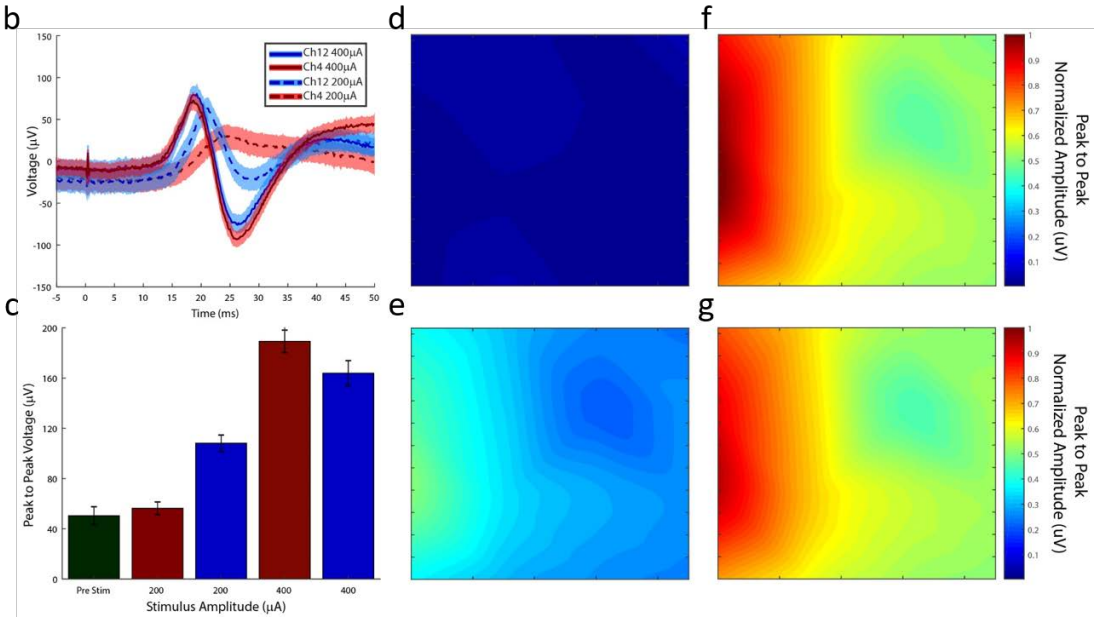

Figure 3.6. *In vivo* acute stimulation results. (**a**) Illustration of *in vivo* acute implantation of CASE and ECoG. (**b**) Somatosensory evoked potential (SSEP) from somatosensory cortex of rat. (**c**) Statistical results of peak to peak potential of SSEP. Heat maps of the SSEP responses (**d**) at channel 4 with 200 µA, (**e**) at channel 12 with 200 µA, (**f**) at channel 4 with 400 µA and (**g**) at channel 12 with 400 µA.

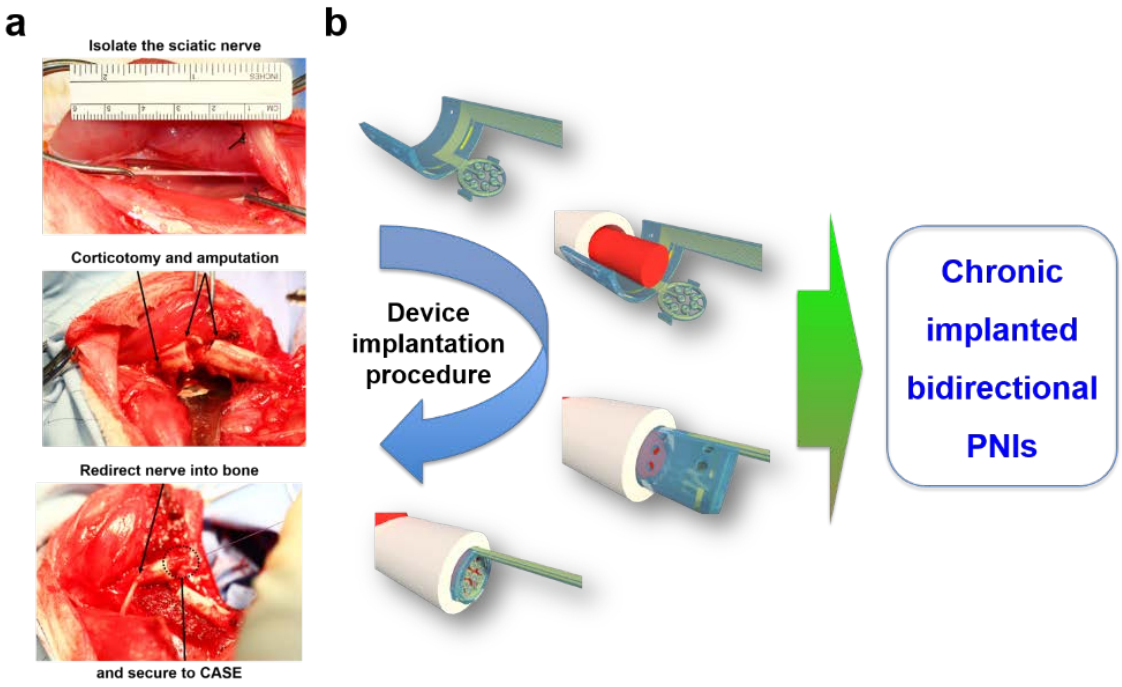

Figure 3.7. Chronic implantation of CASE as a future work. (**a**) surgical model of novel device implantation method. (**b**) Illustration of surgical procedure using CASE.

Chapter 4

Conclusion & Future Directions

There are at least 1.6 million people living with limb loss in the United States and an estimated 185,000 new cases occur each year. The number of Americans living with major limb loss is increasing, and expected to double by 2050[7]. While these numbers do not compare to those with cancer or heart disease, they are still quite staggering when one considers the drastic loss in function and quality of life these individuals are forced to endure for their remaining years. To date prosthetics do not adequately replace the function of the lost limb. Hence, the creation of a novel neural interface is essential for developing the full potential of advanced prosthesis technology required to replace lost limbs in the future. In addition to the prosthetic device development, we focused on the single neuronal cell analysis to get a better understanding of fundamental molecular and cellular mechanisms. This single neuronal cell analysis enables the dynamic study of living neurons can increase the understanding of the interconnecting molecular events continually taking place in each neuron. Each neuron is more or less different from the other, even within the same cell type. Also, meticulous studies of the single neuron and between neurons should be made to explain fundamental biological phenomena such as cellular processes and heterogeneities. Likewise, it has a synergistic effect on neural interface technology when basic research and development of novel neural interfaces are done together.

Utilizing a cellular level approach, we have presented an advanced single-neuronal cell culture and monitoring platform which enables single-neurons to be positioned at a desired location. Further, we conducted real-time live-cell imaging within a controlled

environment to monitor the outgrowth of neurons while preventing exposure of the neuronal cells to hostile environments. Finite element simulation was used to guide the appropriate design parameters and verify the two-dimensional model of the proposed structures. Following fabrication of the device, we demonstrated the capability to trap individual neurons on specific target electrodes with our DEP device. Changes in cell morphology, such as neurite outgrowth, were accurately observed through the transparent substrate in phase contrast, while avoiding photodamage to neurons that often accompanies fluorescent imaging. Importantly, the applied electric field for DEP did not adversely affect cell health, as demonstrated by live-cell imaging and immunolabelled images. Additionally, the accessibility of neurons appropriately grown on the MEAs makes it possible to record the electrical activity of multiple neurons at the same time, and to investigate the electrical communication between them. Therefore, DEP using MEAs allows not only a label-free and non-destructive technique for cell manipulation but also a non-invasive interface with biological cells for long-term (days to weeks) monitoring of electrophysiological parameters[32,45,46]. Thus, the proposed advanced platform has great potential to form an *in vitro* ordered neuronal network and furthers novel and detailed studies of cellular physiology.

As a higher level research, we have demonstrated the fabrication of a novel thin-film peripheral nerve interface combining both traditional cuff and sieve electrode (CASE) interfaces with the capacity to act in both an intraneural and extraneural capacity. Generation of somatosensory evoked potentials generated through the CASE viability of electrical stimulation and bi-directional communication with CASE neural electrodes implanted in rats. Animal experiments incorporating CASE may be carried out over various

time scales from hours to years, as long-term recording or behavioral tests may be performed with a chronically implanted device as shown in Fig. 3.7. Long-term recording with a chronically implanted CASE to quantify the impact on regenerated nerves is on-going. These applications would further validate the use of CASE electrode technology into potential clinical applications. Lastly, the use of this technology with CASE will create a multi-modal platform for investigating the mechanisms of neuromodulation in various neurological disorders.

The theoretical and experimental results presented in this thesis form the inception of the development of novel neural interface. New ways to investigate both cell properties and the phenomenon of electroporation using electrokinetic methods and bi-directional interfacing in the peripheral nervous system were developed that can be exploited in future research linking biology to technology.

References

1. Eggermont, J. J. The correlative brain. In: *The correlative brain* (ed^(eds). Springer (1990).

2. Lisberger, S. & Sejnowski, T. Motor learning in a recurrent network model based on the vestibulo–ocular reflex. *Nature* **360**, 159 (1992).

3. Nicholls, J. G., Martin, A. R., Wallace, B. G. & Fuchs, P. A. *From neuron to brain*. (Sinauer Associates Sunderland, MA, 2001).

4. Jasper, H. H. History of the early development of electroencephalography and clinical neurophysiology at the Montreal Neurological Institute: the first 25 years 1939-1964. *Canadian journal of neurological sciences* **18**, 533-548 (1991).

5. Leuthardt, E. C., Schalk, G., Wolpaw, J. R., Ojemann, J. G. & Moran, D. W. A brain–computer interface using electrocorticographic signals in humans. *Journal of neural engineering* **1**, 63 (2004).

6. Stieglitz, T. & Meyer, J.-U. Cuff electrode. (ed^(eds). Google Patents (1999).

7. Ziegler-Graham, K., MacKenzie, E. J., Ephraim, P. L., Travison, T. G. & Brookmeyer, R. Estimating the Prevalence of Limb Loss in the United States: 2005 to 2050. *Archives of Physical Medicine and Rehabilitation* **89**, 422-429 (2008).

8. Ciardelli, G. & Chiono, V. Materials for peripheral nerve regeneration. *Macromolecular bioscience* **6**, 13-26 (2006).

9. Nicolelis, M. A. Actions from thoughts. *Nature* **409**, 403 (2001).

10. Prochazka, A., Mushahwar, V. K. & McCreery, D. B. Neural prostheses. *The Journal of physiology* **533**, 99-109 (2001).

11. Schanne, O. F., Lavallee, M., Laprade, R. & Gagne, S. Electrical properties of glass microelectrodes. *Proceedings of the IEEE* **56**, 1072-1082 (1968).

12. Robinson, D. A. The electrical properties of metal microelectrodes. *Proceedings of the IEEE* **56**, 1065-1071 (1968).

13. Wheeler, B. C. & Heetderks, W. J. A comparison of techniques for classification of multiple neural signals. *IEEE Transactions on Biomedical Engineering*, 752-759 (1982).

14. Blainey, P. C. & Quake, S. R. Dissecting genomic diversity, one cell at a time. *Nature methods* **11**, 19 (2014).

15. Doron, G. & Brecht, M. What single-cell stimulation has told us about neural coding. *Philos Trans R Soc Lond B Biol Sci* **370**, 20140204 (2015).

16. Konry, T., Sarkar, S., Sabhachandani, P. & Cohen, N. Innovative Tools and Technology for Analysis of Single Cells and Cell-Cell Interaction. *Annu Rev Biomed Eng* **18**, 259-284 (2016).

17. Armbrecht, L. & Dittrich, P. S. Recent Advances in the Analysis of Single Cells. *Anal Chem* **89**, 2-21 (2017).

18. Pohl, H. A. *Dielectrophoresis : the behavior of neutral matter in nonuniform electric fields*. (Cambridge University Press, 1978).

19. Schnelle, T., Müller, T., Voigt, A., Reimer, K., Wagner, B. & Fuhr, G. Adhesion-Inhibited Surfaces. Coated and Uncoated Interdigitated Electrode Arrays in the Micrometer and Submicrometer Range. *Langmuir* **12**, 801-809 (1996).

20. Mittal, N., Rosenthal, A. & Voldman, J. nDEP microwells for single-cell patterning in physiological media. *Lab Chip* **7**, 1146-1153 (2007).

21. Pohl, H. A. & Hawk, I. Separation of Living and Dead Cells by Dielectrophoresis. *Science* **152**, 647-649 (1966).

22. Jones, T. B. *Electromechanics of particles*. (Cambridge University Press, 1995).

23. Pethig, R. Review article-dielectrophoresis: status of the theory, technology, and applications. *Biomicrofluidics* **4**, 022811 (2010).

24. Gray, D. S., Tan, J. L., Voldman, J. & Chen, C. S. Dielectrophoretic registration of living cells to a microelectrode array. *Biosens. Bioelectron.* **19**, 771-780 (2004).

25. Khoshmanesh, K., Nahavandi, S., Baratchi, S., Mitchell, A. & Kalantar-zadeh, K. Dielectrophoretic platforms for bio-microfluidic systems. *Biosens. Bioelectron.* **26**, 1800-1814 (2011).

26. Pohl, H. A., Pollock, K. & Crane, J. S. Dielectrophoretic force: A comparison of theory and experiment. *J. Biol. Phys.* **6**, 133-160 (1978).

27. Bocchi, M., *et al.* Dielectrophoretic trapping in microwells for manipulation of single cells and small aggregates of particles. *Biosens. Bioelectron.* **24**, 1177-1183 (2009).

28. Gross, G. W., Rieske, E., Kreutzberg, G. W. & Meyer, A. A new fixed-array multi-microelectrode system designed for long-term monitoring of extracellular single unit neuronal activity in vitro. *Neurosci. Lett.* **6**, 101-105 (1977).

29. Jaber, F. T., Labeed, F. H. & Hughes, M. P. Action potential recording from dielectrophoretically positioned neurons inside micro-wells of a planar microelectrode array. *J. Neurosci. Methods* **182**, 225-235 (2009).

30. Heida, T., Rutten, W. L. C. & Marani, E. Dielectrophoretic trapping of dissociated fetal cortical rat neurons. *IEEE Trans. Biomed. Eng.* **48**, 921-930 (2001).

31. Yu, Z., *et al.* Negative Dielectrophoretic Force Assisted Construction of Ordered Neuronal Networks on Cell Positioning Bioelectronic Chips. *Biomed. Microdevices* **6**, 311-324 (2004).

32. Maher, M., Pine, J., Wright, J. & Tai, Y.-C. The neurochip: a new multielectrode device for stimulating and recording from cultured neurons. *J. Neurosci. Methods* **87**, 45-56 (1999).

33. Morgan, H. & Green, N. G. *AC Electrokinetics: Colloids and Nanoparticles*. (Research Studies Press, 2003).

34. Allsopp, D. & Betts, W. Dielectrophoretic sensors for microbiological applications. *Selected Topics in Advanced Solid State and Fibre Optic Sensors* **11**, 165 (2000).

35. Kaler, K. V. & Jones, T. B. Dielectrophoretic spectra of single cells determined by feedback-controlled levitation. *Biophysical Journal* **57**, 173-182 (1990).

36. Heida, T., Rutten, W. & Marani, E. Understanding dielectrophoretic trapping of neuronal cells: modelling electric field, electrode-liquid interface and fluid flow. *Journal of physics D: applied physics* **35**, 1592 (2002).

37. Marszalek, P., Liu, D. & Tsong, T. Y. Schwan equation and transmembrane potential induced by alternating electric field. *Biophysical journal* **58**, 1053-1058 (1990).

38. Xia, Y. & Whitesides, G. M. Soft Lithography. *Angew. Chem. Int. Ed.* **37**, 550-575 (1998).

39. Duffy, D. C., McDonald, J. C., Schueller, O. J. A. & Whitesides, G. M. Rapid Prototyping of Microfluidic Systems in Poly(dimethylsiloxane). *Anal. Chem.* **70**, 4974-4984 (1998).

40. Viesselmann, C., Ballweg, J., Lumbard, D. & Dent, E. W. Nucleofection and primary culture of embryonic mouse hippocampal and cortical neurons. *J. Vis. Exp.* **47**, e2373 (2011).

41. Pinto, T. M., Wedemann, R. S. & Cortez, C. M. Modeling the electric potential across neuronal membranes: the effect of fixed charges on spinal ganglion neurons and neuroblastoma cells. *PLoS One* **9**, e96194 (2014).

42. Zhou, T., Perry, S. F., Ming, Y., Petryna, S., Fluck, V. & Tatic-Lucic, S. Separation and assisted patterning of hippocampal neurons from glial cells using positive dielectrophoresis. *Biomed. Microdevices* **17**, 62 (2015).

43. De Lima, A. D., Merten, M. D. & Voigt, T. Neuritic differentiation and synaptogenesis in serum-free neuronal cultures of the rat cerebral cortex. *J. Comp. Neurol.* **382**, 230-246 (1997).

44. Govek, E.-E., Newey, S. E. & Van Aelst, L. The role of the Rho GTPases in neuronal development. *Genes Dev.* **19**, 1-49 (2005).

45. Wang, X. B., Huang, Y., Wang, X., Becker, F. F. & Gascoyne, P. R. Dielectrophoretic manipulation of cells with spiral electrodes. *Biophys. J.* **72**, 1887-1899 (1997).

46. Spira, M. E. & Hai, A. Multi-electrode array technologies for neuroscience and cardiology. *Nat. Nanotechnol.* **8**, 83-94 (2013).

47. Fisher, L. E., Tyler, D. J., Anderson, J. S. & Triolo, R. J. Chronic stability and selectivity of four-contact spiral nerve-cuff electrodes in stimulating the human femoral nerve. *Journal of Neural Engineering* **6**, 046010 (2009).

48. Wang, W., *et al.* Neural interface technology for rehabilitation: exploiting and promoting neuroplasticity. *Physical Medicine and Rehabilitation Clinics* **21**, 157-178 (2010).

49. Hoffer, J. A. & Loeb, G. E. Implantable electrical and mechanical interfaces with nerve and muscle. *Annals of Biomedical Engineering* **8**, 351-360 (1980).

50. Johnston, T. E., Betz, R. R., Smith, B. T. & Mulcahey, M. J. Implanted functional electrical stimulation: an alternative for standing and walking in pediatric spinal cord injury. *Spinal Cord* **41**, 144 (2003).

51. Micera, S. & Navarro, X. Bidirectional interfaces with the peripheral nervous system. *International review of neurobiology* **86**, 23-38 (2009).

52. Brushart, T. M. Central course of digital axons within the median nerve of Macaca mulatta. *Journal of Comparative Neurology* **311**, 197-209 (1991).

53. Branner, A., Stein, R. B. & Normann, R. A. Selective stimulation of cat sciatic nerve using an array of varying-length microelectrodes. *Journal of neurophysiology* **85**, 1585-1594 (2001).

54. Peters, A., Palay, S. L. & Webster, H. d. *The fine structure of the nervous system: neurons and their supporting cells*. (Oxford University Press New York, 1991).

55. Boretius, T., *et al.* A transverse intrafascicular multichannel electrode (TIME) to interface with the peripheral nerve. *Biosensors and Bioelectronics* **26**, 62-69 (2010).

56. Branner, A., Stein, R. B., Fernandez, E., Aoyagi, Y. & Normann, R. A. Long-term stimulation and recording with a penetrating microelectrode array in cat sciatic nerve. *IEEE transactions on biomedical engineering* **51**, 146-157 (2004).

57. Negredo, P., Castro, J., Lago, N., Navarro, X. & Avendaño, C. Differential growth of axons from sensory and motor neurons through a regenerative electrode: a stereological, retrograde tracer, and functional study in the rat. *Neuroscience* **128**, 605-615 (2004).

58. Xavier, N., B., K. T., Natalia, L., Silvestro, M., Thomas, S. & Paolo, D. A critical review of interfaces with the peripheral nervous system for the control of neuroprostheses and hybrid bionic systems. *Journal of the Peripheral Nervous System* **10**, 229-258 (2005).

59. Matthew, S., Daniel, T., Steven, M. S. & Dustin, J. T. Sensory feedback by peripheral nerve stimulation improves task performance in individuals with upper limb loss using a myoelectric prosthesis. *Journal of Neural Engineering* **13**, 016001 (2016).

60. MacEwan, M. R., Zellmer, E. R., Wheeler, J. J., Burton, H. & Moran, D. W. Regenerated Sciatic Nerve Axons Stimulated through a Chronically Implanted Macro-Sieve Electrode. *Frontiers in Neuroscience* **10**, (2016).

61. Belkas, J. S., Shoichet, M. S. & Midha, R. Peripheral nerve regeneration through guidance tubes. *Neurological Research* **26**, 151-160 (2004).

62. Nunamaker, E. A., *et al.* Implantation methodology development for tissue-engineered-electronic-neural-interface (TEENI) devices. In: *2017 8th International IEEE/EMBS Conference on Neural Engineering (NER)* (ed^(eds) (2017).

63. Micera, S., *et al.* On the use of longitudinal intrafascicular peripheral interfaces for the control of cybernetic hand prostheses in amputees. *IEEE Transactions on Neural Systems and Rehabilitation Engineering* **16**, 453-472 (2008).

64. Badia, J., Boretius, T., Andreu, D., Azevedo-Coste, C., Stieglitz, T. & Navarro, X. Comparative analysis of transverse intrafascicular multichannel, longitudinal intrafascicular and multipolar cuff electrodes for the selective stimulation of nerve fascicles. *Journal of neural engineering* **8**, 036023 (2011).

65. Dhillon, G. S. & Horch, K. W. Direct neural sensory feedback and control of a prosthetic arm. *IEEE transactions on neural systems and rehabilitation engineering* **13**, 468-472 (2005).

66. Stieglitz, T., Beutel, H. & Meyer, J.-U. A flexible, light-weight multichannel sieve electrode with integrated cables for interfacing regenerating peripheral nerves. *Sensors and Actuators A: Physical* **60**, 240-243 (1997).

67. Navarro, X., Krueger, T. B., Lago, N., Micera, S., Stieglitz, T. & Dario, P. A critical review of interfaces with the peripheral nervous system for the control of neuroprostheses and hybrid bionic systems. *Journal of the Peripheral Nervous System* **10**, 229-258 (2005).

68. Lago, N., Udina, E., Ramachandran, A. & Navarro, X. Neurobiological assessment of regenerative electrodes for bidirectional interfacing injured peripheral nerves. *IEEE transactions on biomedical engineering* **54**, 1129-1137 (2007).

69. Garde, K., Keefer, E., Botterman, B., Galvan, P. & Romero-Ortega, M. I. Early interfaced neural activity from chronic amputated nerves. *Frontiers in neuroengineering* **2**, 5 (2009).

70. FitzGerald, J. J., *et al.* A regenerative microchannel neural interface for recording from and stimulating peripheral axons in vivo. *Journal of neural engineering* **9**, 016010 (2012).

71. Minev, I. R., Chew, D. J., Delivopoulos, E., Fawcett, J. W. & Lacour, S. P. High sensitivity recording of afferent nerve activity using ultra-compliant microchannel electrodes: an acute in vivo validation. *Journal of neural engineering* **9**, 026005 (2012).

72. Rutten, W. L. Selective electrical interfaces with the nervous system. *Annual review of biomedical engineering* **4**, 407-452 (2002).

73. Gustafson, K. J., Grinberg, Y., Joseph, S. & Triolo, R. J. Human distal sciatic nerve fascicular anatomy: implications for ankle control using nerve-cuff electrodes. *Journal of Rehabilitation Research & Development* **49**, (2012).

74. Delgado-Martínez, I., Badia, J., Pascual-Font, A., Rodríguez-Baeza, A. & Navarro, X. Fascicular Topography of the Human Median Nerve for Neuroprosthetic Surgery. *Frontiers in Neuroscience* **10**, (2016).

75. Kawada, T., Zheng, C., Tanabe, S., Uemura, T., Sunagawa, K. & Sugimachi, M. A sieve electrode as a potential autonomic neural interface for bionic medicine. In: *The 26th Annual International Conference of the IEEE Engineering in Medicine and Biology Society* (ed^(eds) (2004).

76. Thompson, C. H., Zoratti, M. J., Langhals, N. B. & Purcell, E. K. Regenerative electrode interfaces for neural prostheses. *Tissue Engineering Part B: Reviews* **22**, 125-135 (2015).

77. Park, D.-W., *et al.* Fabrication and utility of a transparent graphene neural electrode array for electrophysiology, in vivo imaging, and optogenetics. *Nature protocols* **11**, 2201 (2016).

78. Park, D.-W., *et al.* Graphene-based carbon-layered electrode array technology for neural imaging and optogenetic applications. *Nature Communications* **5**, 5258 (2014).

79. Gesteland, R. C., Howland, B., Lettvin, J. Y. & Pitts, W. H. Comments on microelectrodes. *Proceedings of the IRE* **47**, 1856-1862 (1959).

80. Park, D.-W., *et al.* Electrical Neural Stimulation and Simultaneous in Vivo Monitoring with Transparent Graphene Electrode Arrays Implanted in GCaMP6f Mice. *ACS Nano* **12**, 148-157 (2018).

81. Schendel, A. A., *et al.* A cranial window imaging method for monitoring vascular growth around chronically implanted micro-ECoG devices. *Journal of neuroscience methods* **218**, 121-130 (2013).

82. Schendel, A. A., *et al.* The effect of micro-ECoG substrate footprint on the meningeal tissue response. *Journal of neural engineering* **11**, 046011 (2014).

83. Cogan, S. F. Neural stimulation and recording electrodes. *Annu. Rev. Biomed. Eng.* **10**, 275-309 (2008).

84. Norlin, P., Kindlundh, M., Mouroux, A., Yoshida, K. & Hofmann, U. G. A 32-site neural recording probe fabricated by DRIE of SOI substrates. *Journal of Micromechanics and Microengineering* **12**, 414 (2002).

85. Williams, J. C., Hippensteel, J. A., Dilgen, J., Shain, W. & Kipke, D. R. Complex impedance spectroscopy for monitoring tissue responses to inserted neural implants. *Journal of neural engineering* **4**, 410 (2007).

86. Tan, D. W., Schiefer, M. A., Keith, M. W., Anderson, J. R., Tyler, J. & Tyler, D. J. A neural interface provides long-term stable natural touch perception. *Science translational medicine* **6**, 257ra138-257ra138 (2014).